Eur. Phys. J. A (2025) 61:28
https://doi.org/10.1140/epja/s10050-025-01491-y

THE EUROPEAN PHYSICAL JOURNAL A

Regular Article - Theoretical Physics

Isovector properties of effective finite-range nuclear interactions

D. Davesne[1,2,3,a], **J. Navarro**[4,b], **A. Pastore**[5,c], **Y. Lallouet**[6]

[1] Université de Lyon, Lyon 69003, France
[2] Université Lyon 1, 43 Bd. du 11 Novembre 1918, Villeurbanne Cedex 69622, France
[3] CNRS-IN2P3, UMR 5822, Institut de Physique Nucléaire de Lyon, Lyon, France
[4] IFIC (CSIC-Universidad de Valencia), Parque Científico, Catedrático José Beltrán 2, 46980 Paterna, Spain
[5] CEA, DES, IRESNE, DER, SPRC, Saint Paul Lez Durance 13108, France
[6] Lycée Malherbe, 14, Avenue Albert Sorel, 14000 Caen, France

Received: 24 July 2024 / Accepted: 16 January 2025

Communicated by Takashi Nakatsukasa

Abstract We discuss several properties of two families of finite-range interactions in infinite nuclear matter, aiming in particular to their isovector properties. We find that the recent parameterisations of both Gogny and Nakada provide a reasonable description of the properties of the infinite medium as well as an equation of state capable of sustaining a two solar mass neutron star. We also discuss the pairing properties in the spin-singlet channel for both families of interactions.

1 Introduction

The use of mean-field methods based on the effective nucleon-nucleon (NN) interaction is very popular in the nuclear physics community [1], since it allows a variety of nuclear observables to be reproduced with good accuracy all along the nuclear chart [2]. According to their radial form factor, we define three main families of effective interactions used for this purpose: the Skyrme [3], characterised by a zero-range form factor, and the Gogny [4] and Nakada [5], which have a finite range. We recall that a finite range is important to avoid spurious truncations in the pairing channels within Hartree-Fock-Bogoliubov (HBF) calculations [6], as a consequence one can use the same interaction for both particle-hole and particle-particle sector. Besides, using finite range interactions can help to be in touch, at least qualitatively, with realistic interactions. Regardless of the type of interaction, they are all characterised by some adjustable parameters that must be determined by a well-defined fitting protocol [7].

There is no unique way to define such a protocol: different groups use different observables and weights to define their penalty function [8]. However, it is possible to see that the vast majority of these fits include some properties of infinite nuclear matter (INM), which we assume to be spin-saturated. Symmetric (SNM) and asymmetric (ANM) nuclear matter are uniquely characterised by their density and isospin imbalance. Although such a model can be considered as an over-simplification, it is capable of describing some features of massive compact objects such as neutron stars [9]. It is also possible to use it to compare the results obtained at the mean-field level with more sophisticated tools such as *ab-initio* methods [10]. Thanks to all this information, it is possible to better constrain the effective NN interactions, especially in the case of large isospin asymmetry, in order to have a better predictive power when used to describe nuclei close to drip lines [11]. For all these reasons it is important to study in detail the properties of INM with effective interactions. The case of Gogny interactions was addressed in Ref. [12], where it was shown that, using the set of eleven Gogny interactions available at that time, there is a large variation in the isospin properties. In particular, the predicted density dependence of the symmetry energy is too soft and lies outside the currently accepted values. The authors also showed that most of the parameterisations are not applicable to astrophysical calculations.

In this work, we have decided to repeat part of the analysis carried out in Ref. [12], but focusing on the Nakada interactions with the aim of studying their isovector properties. We will present analytical results for some quantities relevant to astrophysics, such as the symmetry energy and its slope, as well as the general equation of state of hadronic matter. We have chosen to follow the notations given in Ref. [12] to facilitate the comparison between the results obtained from the

[a] e-mail: davesne@ipnl.in2p3.fr
[b] e-mail: navarro@ific.uv.es
[c] e-mail: alessandro.pastore@cea.fr (corresponding author)

Published online: 07 February 2025

Gogny and Nakada interactions. We also include in the current article the new Gogny interactions with a *non-standard* central term [4] in order to test their applicability in astrophysical scenarios. The systematic comparison between the two families of interactions will then provide a better insight into the role of the radial form factor, but also into the flexibility of the model in simultaneously reproducing INM and finite nuclei properties.

The article is structured as follows: in Sect. 2 we introduce the interactions considered in this paper. In Sect. 3 we discuss the main features of asymmetric nuclear matter obtained with these interactions, and in Sect. 4 we study the pairing properties. Finally, in Sect. 5 we present our conclusions.

2 Interactions

In the present work, we perform Hartree-Fock (HF) calculations using an uncoupled basis in an infinite homogeneous system. This allows us to write only the central and density dependent part of each interaction, since the tensor and spin-orbit terms do not contribute [13,14].

The Nakada interaction is derived from the so-called Michigan three-range Yukawa (M3Y) interaction [15], which was originally constructed by fitting its matrix elements, calculated in an oscillator basis, to the G-matrix elements calculated with realistic NN potentials such as Reid [15] and Paris [16]. The M3Y interaction was designed for inelastic nucleon-nucleus scattering studies and failed to reproduce the saturation point of symmetric nuclear matter [17]. Density-dependent coupling constants have been introduced to remedy this failure and applied to the study of nucleon-nucleon scattering [18,19] in the folding model. However, these extensions give unsatisfactory results in finite nuclei, especially for saturation and spin-orbit splitting. For more details on the INM properties of these additional interactions, we refer to Refs. [20,21].

In a series of papers, Nakada defined a new extension, also starting from a M3Y parameterisation, whose G-matrix was obtained from the Paris NN interaction [16], including both tensor and spin-orbit terms, and adding an explicit Skyrme-like density-dependent term to properly account for INM saturation properties as well as various ground state properties of finite nuclei. The long-range part of the original M3Y interaction was retained, so that the main features of the one-pion exchange potential (OPEP) are asymptotically fulfilled. Various optimisations of the interaction parameters have led to the M3Y-Pn family of semi-realistic NN interactions [5,22–24]. These interactions are able to satisfy basic constraints in INM, such as saturation, and also provide a reasonable description of various properties of atomic nuclei [25–27]. A recent paper [28] also shows that these interactions can be used to calculate differential cross sections with reasonable accuracy.

The general Nakada interaction [5] (central part) takes the form

$$\begin{aligned} V_{\text{Nakada}}(r) = {} & t_0(1+x_0P_\sigma)\rho^\gamma\delta(r) + t_\rho^{SE}P_{SE}\rho^{\gamma_{SE}}\delta(r) \\ & + t_\rho^{TE}P_{TE}\rho^{\gamma_{TE}}\delta(r) \\ & + \sum_i \left(t_i^{SE}P_{SE} + t_i^{TE}P_{TE} + t_i^{SO}P_{SO}\right. \\ & \left. + t_i^{TO}P_{TO}\right)\frac{1}{r\mu_i}\mathrm{e}^{-r\mu_i}. \end{aligned} \tag{1}$$

In fact, the first density-dependent term in this equation corresponds to the first version of the interaction (M3Y-P2), while more recently it has been replaced by two separate contributions in the singlet-even (SE) and triplet-even (TE) channels, which are the second and third terms in Eq. (1). We start from the above general expression in order to include the existing parameterisations in the general expressions derived along this paper. This interaction is characterised by three ranges $\mu^{-1} = 0.25, 0.4, 1.414$ fm corresponding to the Compton wavelengths of mesons with masses of 790, 490 and 140 MeV respectively. Contrary to the case of Gogny, where we observe a certain variance in the adopted ranges, Nakada kept them fixed for all the optimisations.

As in the Gogny case, the Nakada interaction is the same in the particle-hole and particle-particle channels to account for nuclear superfluidity [29]. This is an additional constraint to take into account when fitting the coupling constants of the interaction. This is not the case for typical Skyrme interactions [3], where two different interactions are used in these channels.

As anticipated in the introduction, we want to compare the Nakada M3Y-Pn results with some recent Gogny parameterisations. As typical examples of Gogny interactions, we have chosen D1 [4] and D1P [30] and four recent ones such as D1M* [31], D2 [32], D3G3 [33] and D3G3M [34], which were not considered in Ref. [12]. These parameterisations have been adjusted to improve the properties of the INM, especially in view of astrophysical applications. The interest of these interactions is that they differ not only in the fitting protocol, but also in the structure of the central term. For example, D1P has two zero-range density dependent terms, D2 has one finite range density dependent term, while D3G3 and D3G3M have three ranges instead of the canonical two.

Since the Nakada interaction already contains three ranges and two independent density dependent terms, it already has a structure that is richer than the standard *Gogny* such as D1, and as such, we expect to be able to obtain INM results comparable to the extended Gogny interactions.

Within the HF approach to INM, the coupling constants appear under specific combinations which, following the notation of Ref. [12], we write with the letters A, B for the

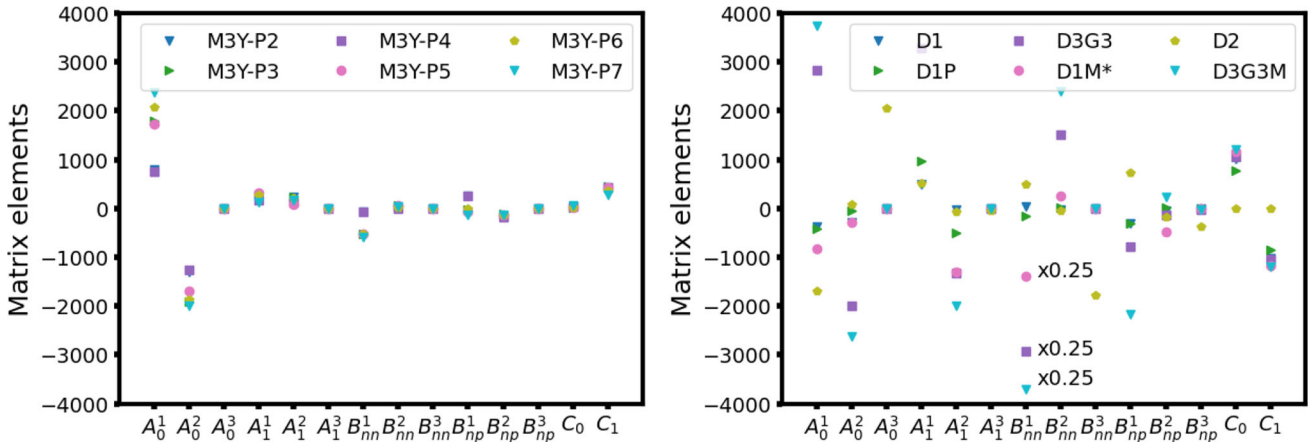

Fig. 1 Relevant combinations of interaction parameters. The left (right) panel shows the matrix elements of various Nakada (Gogny) interactions. Note that the B_{nn}^1 matrix element of D1M*, D3G3 and D3G3M has been divided by a factor of 4 to fit the scale of the plot. The units are [MeV fm^3] for A, [MeV] for B and [MeV fm$^{3\gamma+3}$] for C

direct and exchange terms of the finite-range part of the interaction, respectively, and with the letter C for the zero-range one. Their explicit expressions are

$$A_0^i = \frac{\pi}{4\mu_i^3}(3t_i^{(SE)} + 3t_i^{(TE)} + t_i^{(SO)} + 9t_i^{(TO)}), \tag{2}$$

$$A_1^i = \frac{\pi}{4\mu_i^3}(t_i^{(SE)} - 3t_i^{(TE)} - t_i^{(SO)} + 3t_i^{(TO)}), \tag{3}$$

$$B_{nn}^i = \frac{1}{16\pi}(t_i^{SE} - 3t_i^{TO}), \tag{4}$$

$$B_{np}^i = \frac{1}{32\pi}(t_i^{SE} + 3t^{TE} - t_i^{TSO} - 3t_i^{TO}), \tag{5}$$

$$C_0 = \frac{3}{4}t_0, \tag{6}$$

$$C_1 = -\frac{1}{4}t_0(1 + 2x_0), \tag{7}$$

$$C_{SE} = \frac{1}{16}t_\rho^{SE}, \tag{8}$$

$$C_{TE} = \frac{3}{16}t_\rho^{TE}. \tag{9}$$

We define also the combinations

$$B_0^i = B_{nn}^i + B_{np}^i, \tag{10}$$

$$B_1^i = B_{nn}^i - B_{np}^i. \tag{11}$$

Unlike the zero-range case of Skyrme [35], one cannot directly relate the parameters of the interaction to some infinite matter properties. For finite-range interactions, these properties are related to specific linear combinations (as shown above). In Fig. 1, we show the matrix elements for the Nakada M3Y-Pn family (left panel) and Gogny (right panel). The explicit expressions of these quantities for the Gogny interactions are given in Appendix A.

A very striking feature of this comparison is the large variability of the Gogny matrix elements compared to the Nakada ones. The Gogny interactions have been fitted by several groups and many people, using many different ingredients for the fits. Presumably, Nakada has proceeded in a more smooth way. This is why the values of the matrix elements are more concentrated for Nakada (except for A_0, C_1) and more scattered for Gogny. We also note that the terms $A_{0,1}^3$ for the Nakada interactions are zero by construction, and that the same method has been used to fit the third range of D3G3 and D3G3M. Finally, we included in this figure the density-dependent dependent term of the D2 interaction in the A^3, B^3 terms. Due to the presence of a range now the density dependence enter in all combinations of matrix elements and it is no more restricted to the C coefficients only as for the other interactions. We recall that D1P is the only interaction having two explicit density dependences, for simplicity in Fig. 1 we showed just the first one. We give here the explicit values for the second $C_{0(1)}^2 = 192.0\ (192.9)$ [MeVfm$^{3\alpha_2+3}$] respectively.

3 Asymmetric nuclear matter

In asymmetric nuclear matter, we define the isospin asymmetry as

$$\beta = \frac{\rho_n - \rho_p}{\rho}, \tag{12}$$

where $\rho_{n(p)}$ is the density of neutron (protons). The respective Fermi momenta are defined as

$$k_F = \left(\frac{3\pi^2}{2}\rho\right)^{1/3}, \tag{13}$$

$$k_{F\tau} = \left(3\pi^2\rho_\tau\right)^{1/3} = \left(\frac{3\pi^2}{2}\rho[1 + \tau\beta]\right)^{1/3}, \tag{14}$$

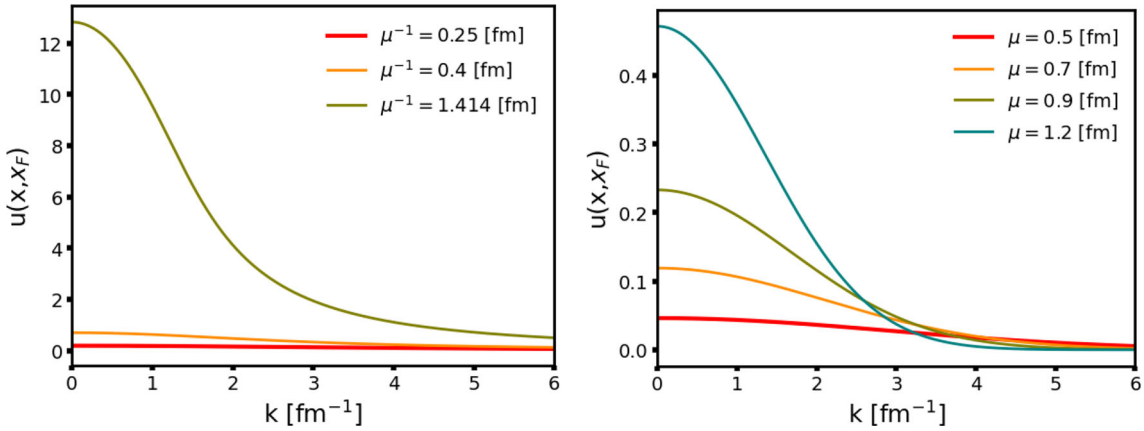

Fig. 2 Functions $\mathrm{u}(x, x_F)$ for different values of μ plotted as a function of momentum at saturation density. Yukawa (left) and Gaussian (right) form factors

with $\tau = +1$ for neutrons and -1 for protons. For the sake of simplicity, we also assume the system saturated in spin and we neglect electromagnetic interactions.

3.1 Mean field potential

We start our analysis by considering the single particle mean field potential

$$U_\tau(\mathbf{k}) = \frac{1}{2}\sum_{\tau'\sigma\sigma'}\int \frac{\mathrm{d}\mathbf{k}'}{(2\pi^3)} \langle \mathbf{k}\sigma\tau;\mathbf{k}'\sigma'\tau'|V(1-P_x P_\sigma P_\tau)|\mathbf{k}\sigma\tau;\mathbf{k}'\sigma'\tau'\rangle, \quad (15)$$

where we have antisymmetrised the matrix elements via the spatial P_x, spin P_σ, and isospin P_τ exchange operators. Since the wavefunctions of the systems are plane waves, this equation can be calculated analytically and we obtain the following expression, written in a general form that is valid for both Nakada and Gogny interactions

$$\begin{aligned} U_\tau(k) = &\sum_i A_0^i\rho + A_1^i\tau\beta\rho \\ &+B_{nn}^i \mathrm{u}(x^i, x_\tau^i) + B_{np}^i \mathrm{u}(x^i, x_{-\tau}^i) \\ &+\left[\frac{1}{2}(2+\gamma)C_0\rho^{\gamma+1} + \left(\tau\beta + \frac{1}{2}\gamma\beta^2\right)C_1\rho^{\gamma+1}\right] \\ &+2C_{SE}\,\rho^{\gamma_{SE}+1}(3+\tau\beta) \\ &+2C_{TE}\,\rho^{\gamma_{TE}+1}(1-\tau\beta)+C_{SE}\,\gamma_{SE}\rho^{\gamma_{SE}+1}(3+\beta^2) \\ &+C_{TE}\,\gamma_{TE}\rho^{\gamma_{TE}+1}(1-\beta^2). \end{aligned} \quad (16)$$

In this equation, we have defined the dimensionless quantities $x^i = k/\mu_i, x_\tau^i = k_{F\tau}/\mu_i$ for Nakada and $x^i = k\mu_i, x_\tau^i = k_{F\tau}\mu_i$ for Gogny. Notice that each form factor uses a parameter μ with a different meaning (range and inverse range). We have maintained their original notation, using a dimensionless parameter x. The whole momentum dependence is contained in the functions $\mathrm{u}(x, x_F)$ and their explicit expression is given in Appendix B. We plot them as a function of k for SNM and several ranges in Fig. 2 at $\rho = 0.16$ [fm^{-3}].

Apart from the obvious difference in absolute scale, one notices that due to the nature of the Yukawa form factor, the $\mathrm{u}(x, x_F)$ functions go to zero relatively slowly compared to the Gogny case. As discussed below, this has a direct impact on the evolution $U_\tau(k)$ for large values of k.

In Fig. 3 we show the momentum dependence of the single particle potential $U_\tau(k)$ for both neutrons and protons at four values of asymmetry $\beta = 0, 0.3, 0.6, 1$. For the proton mean-field, the case $\beta = 1$ should be understood as $\beta \to 1$, which is the limit of proton impurity in neutron matter. All the calculations have been carried out at the saturation density specific to each interaction, given in Tables 1 and 2.

We observe a common trend for all interactions. For SNM ($\beta = 0$) they all lead to similar values of the single-particle potential in the range of momenta from zero to about 2 fm^{-1}. All interactions sensibly give the same value, about –80 MeV at zero momentum. At 2 fm^{-1} the values rise smoothly to –34 MeV for M3Y-P2 to –27 MeV for M3Y-P7. At higher momenta the potential increases, although the interactions M3Y-P2 and M3Y-P4 seem to reach a constant value at about 4 fm^{-1}. For a non-zero isospin asymmetry we observe that at zero momentum the potential values are practically the same for parameterisations M3Y-P2 to M3Y-P5 and become slightly more repulsive for the newer M3Y-P6 and M3Y-P7. It is worth noting that microscopic results for the energy per particle of neutron matter [36,37] were used to fit the latter interactions. In all cases, we observe that as β increases the neutron potential increases while the proton potential decreases, reflecting the fact that in neutron-rich systems neutrons are less bound while protons are more bound. We also notice that asymmetry effects are reduced with increasing momentum, especially for the neutron potential.

In Fig. 4 we show the same quantities for some selected Gogny interactions. As shown in Ref. [12], the existing

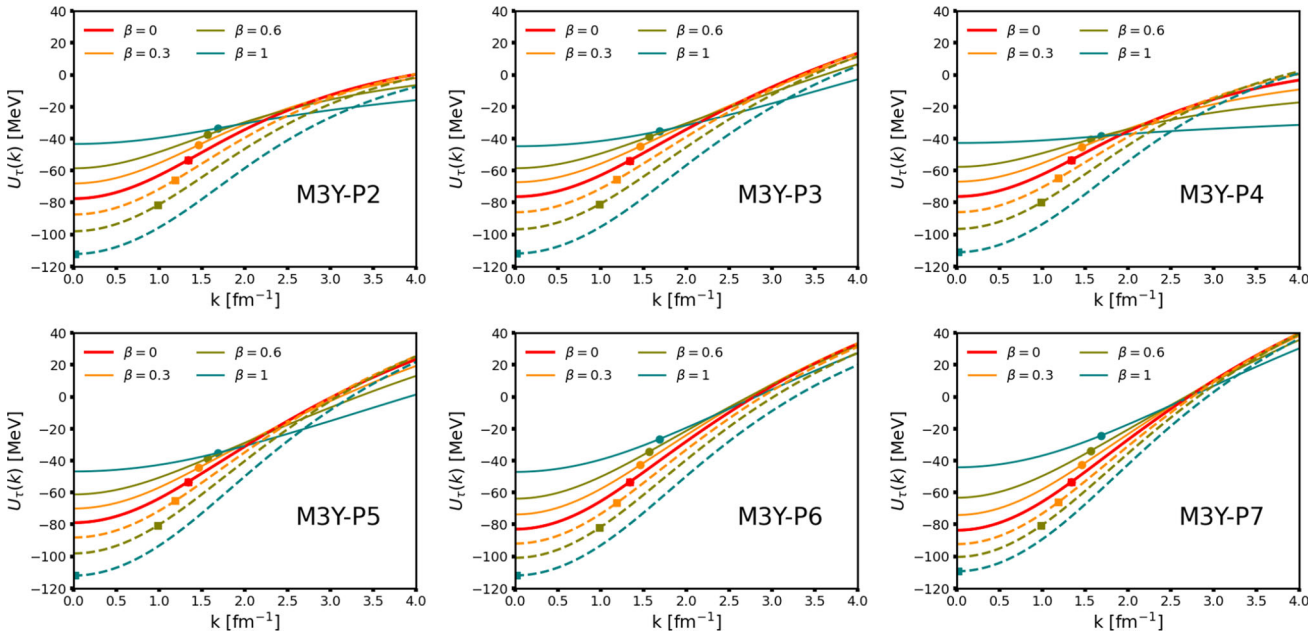

Fig. 3 Single-particle potentials $U_\tau(k)$ for neutrons (solid) and protons (dashed) as a function of the single-particle momentum k at saturation density and different isospin asymmetries for the Nakada interactions considered in this work. The symbols denote the single-particle potential of a neutron (circles) or a proton (square) at the respective Fermi momentum $k_{F\tau}$. See text for details

Table 1 INM properties of Nakada interactions evaluated at saturation density ρ. See text for details

	E/A [MeV]	ρ_0 [fm^{-3}]	m^*/m_N	K_0 [MeV]	Q_0 [MeV]	$S(\rho_0)$ [MeV]	$L(\rho_0)$ [MeV]	$K_{sym}(\rho_0)$[MeV]	$Q_{sym}(\rho_0)$ [MeV]
M3Y-P2	−16.144	0.163	0.652	221	−435	30.6	27.9	−220.6	547.3
M3Y-P3	−16.508	0.163	0.657	247	−367	29.8	25.2	−209.9	573.7
M3Y-P4	−16.135	0.163	0.665	236	−374	28.7	17.8	−230.7	613.4
M3Y-P5	−16.117	0.163	0.629	236	−383	29.6	24.5	−213.5	566.6
M3Y-P6	−16.235	0.163	0.596	240	−379	32.1	44.6	−165.5	459.5
M3Y-P7	−16.224	0.163	0.589	255	−321	31.7	51.5	−127.9	414.9

Table 2 Same as Table 2, but for Gogny

	E/A [MeV]	ρ_0 [fm^{-3}]	m^*/m_N	K_0 [MeV]	Q_0 [MeV]	$S(\rho_0)$ [MeV]	$L(\rho_0)$ [MeV]	$K_{sym}(\rho_0)$[MeV]	$Q_{sym}(\rho_0)$ [MeV]
D1	−16.304	0.166	0.670	230	−462	30.7	18.3	−275.1	618.0
D1P	−15.040	0.169	0.672	250	−336	32.4	49.7	−157.1	404.6
D3G3	−16.048	0.164	0.678	227	−316	32.5	36.7	−131.4	789.6
D3G3M	−16.058	0.164	0.739	240	−292	28.5	25.4	−124.5	813.1
D1M*	−16.058	0.164	0.746	225	−459	30.2	43.1	−47.3	705.7
D2	−15.996	0.163	0.738	209	−427	31.1	44.8	−88.8	666.8

Gogny parameterisations lead to large variations in the isospin properties. In the range of momenta from zero to about 2 fm^{-1}, the potentials show a similar trend as compared to those obtained with Nakada interactions. At zero momentum, Gogny interactions give a value of about –80 MeV ($\beta = 0$). However, for larger momenta we observe that for D1 there is a crossing of the neutron/proton potential at large asymmetry, meaning that neutrons are bound more than protons in very neutron-rich systems. This problem has been recognised and corrected, leading to the D1N parameterisation [38].

Since the momentum functions $\mathrm{u}(x, x_F)$ vanish at $k \to +\infty$, the behavior of the single particle potential at large momentum values is dominated by the direct and density-

dependent parts of the interaction (except for D2). The momentum at which the momentum dependent part of the potential vanishes depends on the interaction: typically for Gogny interactions it is around $k \approx 4/5$ [fm^{-1}], while for Nakada interactions it is around $k \approx 6/8$ [fm^{-1}] (or even higher). It is interesting to observe that also the D3G3 and D3G3M, due to the presence of a very short range, show a non-negligible momentum dependence of the potential up to very high momenta and thus have a comparable behaviour to the M3Y-Pn family.

Regardless of the asymptotic value of $U_\tau(k)$, we find that for the majority of interactions (except D2 and D1M*) the minimum of the single-particle potential occurs at $k = 0$. The special cases of D2 and D1M* together with M3Y-P7 (for comparison) are illustrated in Fig. 5, where we show the evolution of the single particle potential up to larger momenta. Once isospin asymmetry is present, the minimum of the proton potential is shifted to $k \approx 5$ (for D2) or $k \approx 8$ fm^{-1} for D1M*. Such a behavior has not been observed for any other interaction, and although not relevant for simple Hartree-Fock calculations, it may play a role in beyond mean-field calculations of neutron-rich nuclei, revealing a possible pathology of the interactions.

As can be seen from Eq. (16), the single-particle potential is the sum of three contributions: the Hartree (direct), the Fock (exchange) and a density dependent one. Their relative intensities are usually not constrained, since they are not observable, but it is still interesting to observe their relative importance, since this can have an impact on numerical calculations. For most interactions, such as D1, D1P or M3Y-P2, the Hartree term in the SNM at saturation almost cancels out the density dependent one, and thus the main contribution to the single particle comes from the Fock term. For other interactions, such as D2, the Fock term is quite weak and the bulk of the contribution comes from an attractive Hartree plus density dependent term. Finally, another group of interactions such as D3G3, D3G3M, M3Y-P5, M3Y-P6 and M3Y-P7 have a very strong repulsive direct term (of the order of 50 to 200 MeV) and a strong attractive Fock term ($\approx$ –150 to –300 MeV) around $k = 0$, and thus the standard value of $U^\tau(k = 0) \approx -80$ MeV arises from a strong cancellation of these two terms. This situation is quite similar to what happens in relativistic mean field theory [39]. This is not a problem in itself, but this cancellation requires knowledge of the parameters of the interaction up to several digits [33] and also a careful implementation of the numerical solver to avoid large errors when using these interactions.

Following Ref. [12], one can also define an isoscalar U_0 and isovector U_1 potential as[1]

$$\begin{aligned} U_0(k) = &\sum_i A_0^i \rho + B_0^i \mathrm{u}(x^i, x_F^i) \\ &+\frac{1}{2}(2+\gamma) C_0 \rho^{\gamma+1} + 3(2+\gamma_{SE}) C_{SE}\, \rho^{\gamma_{SE}+1} \\ &+(2+\gamma_{TE}) C_{TE}\, \rho^{\gamma_{TE}+1}, \end{aligned} \tag{17}$$

$$\begin{aligned} U_1(k) = &\left.\frac{\partial U_n(k)}{\partial \beta}\right|_{\beta=0} = C_1 \rho^{\gamma+1} + 2C_{SE}\rho^{\gamma_{SE}+1} \\ &-2C_{TE}\rho^{\gamma_{TE}+1} + \sum_i A_1^i \rho + \frac{1}{3} B_1^i\, \mathrm{u}_1(x^i, x_F^i) \end{aligned} \tag{18}$$

We report in Fig. 6 and in Fig. 7 the evolution of these isoscalar and isovector potentials for three values of the density, namely 1/2, 1 and 3/2 of ρ_0 for the Nakada and Gogny interactions. As shown in Fig. 5, we see that the isoscalar potential for D2, and to some extent also for D1M*, exhibits a secondary minimum at high momenta not only at saturation, but also at other values of the density of the system. For the isovector case, we see that all Nakada interactions show a decreasing behavior, while the Gogny interactions, apart D1 and D1P, present an opposite trend. The only constraint we have is represented by the shaded are at $\rho = \rho_0$ panel and it is obtained from Ref. [40] via fits of optical potentials. We see that (apart from the absolute value) the trend derived from the analysis of Ref. [40] is a decreasing potential as k increases, thus in good agreement with what observed for the Nakada interactions.

3.2 Effective mass

The effective mass also provides an important characterisation of the momentum dependence of the single-particle potential. It is obtained as

$$\frac{m}{m_\tau^*} = 1 + \frac{m}{\hbar^2 k}\frac{\partial U_\tau(k)}{\partial k}, \tag{19}$$

where m is the bare nucleon mass, which for simplicity we assume to be the same for protons and neutrons. A straightforward calculation leads to the following expression

$$\begin{aligned} \frac{\hbar^2}{2m_\tau^*(k)} = &\frac{\hbar^2}{2m} + \sum_i d_i^2 \big[B_{nn}^i \mathrm{m}(x^i, x_\tau^i) \\ &+B_{np}^i \mathrm{m}(x^i, x_{-\tau}^i)\big]. \end{aligned} \tag{20}$$

where we defined $d_i = \frac{1}{\mu_i}$ for Nakada and $d_i = \mu_i$ for Gogny. As can be seen by inspecting Eq. (20), the effective mass arises entirely from the momentum dependent part of

[1] Note that in Eqs. A9-A11 of Ref. [12], the rearrangement term is missing.

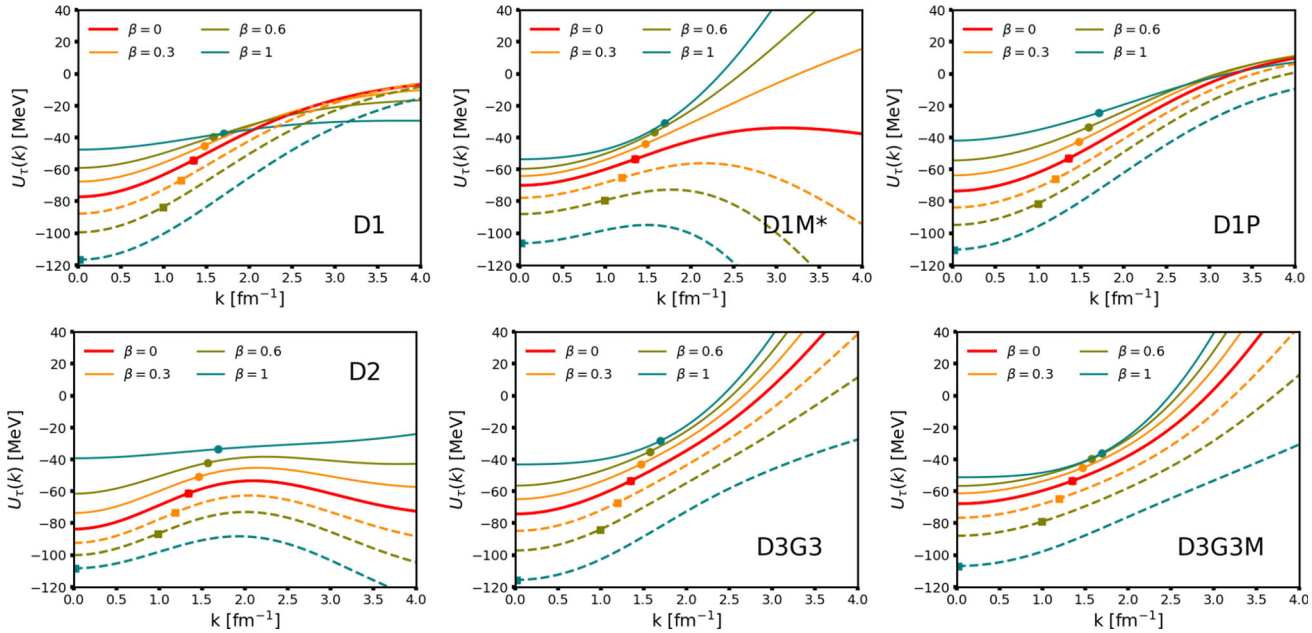

Fig. 4 Same as Fig. 3, but for Gogny interactions

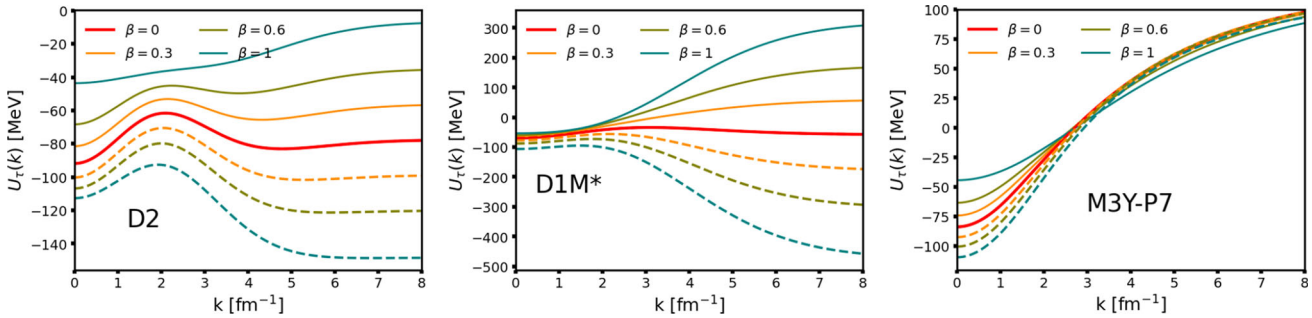

Fig. 5 Same as Fig. 3, but for large values of k and for Gogny D2 (left panel), Gogny D1M* (central panel) and Nakada M3Y-P7 (right panel)

the interaction, and for finite range interactions this dependence is encapsulated in the function $\mathrm{m}(x, x_\tau)$. The explicit expressions are given in Appendix B. In Fig. 8 we show for SNM and saturation density the evolution of this function for Nakada (left) and Gogny (right) as a function of momentum k. We observe that, apart from an obvious scale factor, the $\mathrm{m}(x, x_F)$ functions have a monotonous behavior dropping to zero faster in the case of Gogny than Nakada.

In Figs. 9-10, we show the evolution of the effective mass as a function of the momentum k for selected Nakada and Gogny interactions and 4 values of isospin asymmetry, going from SNM ($\beta = 0$) to pure neutron matter (PNM) ($\beta = 1$). As in the case of the single particle potential, we observe quite a variety of behaviors. A common feature of the Nakada interactions is that neutrons have a larger effective mass than protons, which is also the case for D1 and D1P. For the most recent Gogny interactions on the contrary, an inversion is observed around k_F for D1M* and slightly above for D2, D3G3 and D3G3M. This region is not relevant for finite nuclei, but it may play a role in some astrophysical calculations such as the neutrino mean free path as discussed in Ref. [41].

Most of the interactions have been constrained using SNM at saturation density to obtain a value of $m^*/m_N \approx 0.6-0.7$, and we observe that both families of interactions respect such a constraint, but with a very different momentum dependence. In the case of Nakada we observe a monotonous behavior with all values of the effective mass converging to m_N at large momenta, while in the case of Gogny we observe a variety of behaviors still converging to m_N at large momenta, but with crossings and inversions depending on β. No firm conclusions can be drawn, since the exact structure of the momentum dependence of the effective mass is not fully known. Some results are available from Brueckner-Hartree-Fock (BHF) calculations, but only for a limited range of densities and asymmetries. See Ref. [42] for a recent review on this topic.

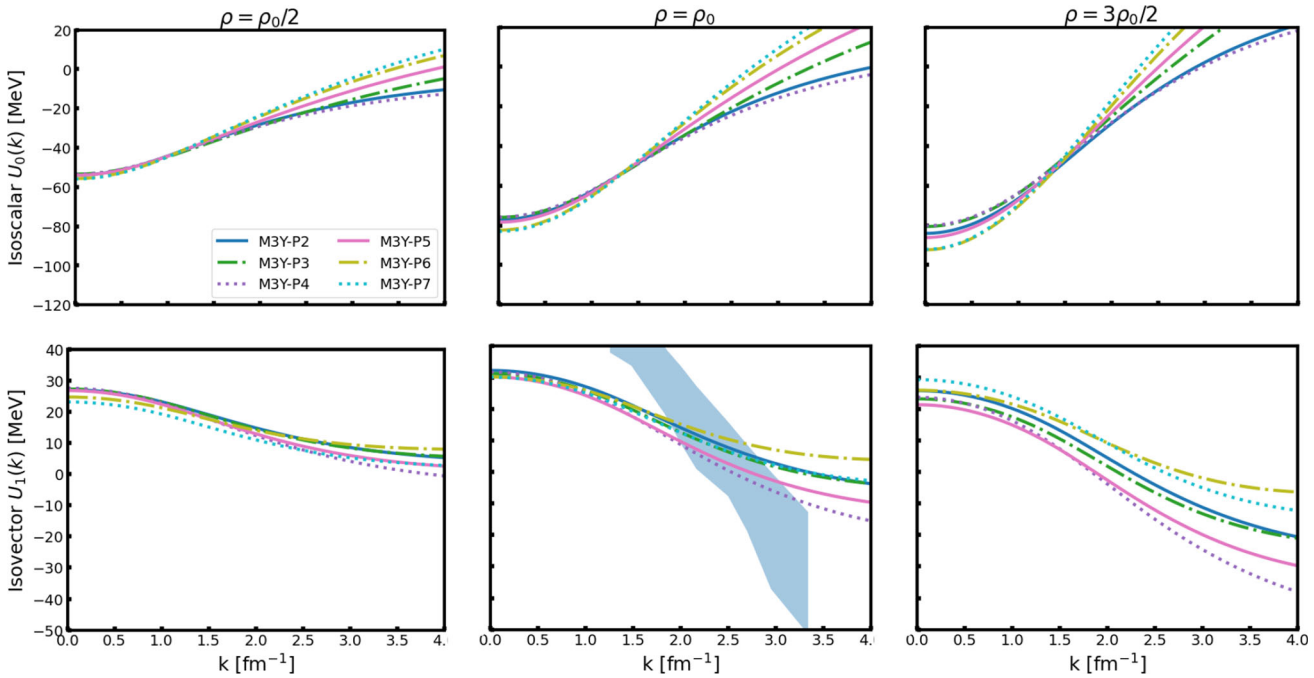

Fig. 6 Isoscalar and isovector potentials for Nakada interactions as a function of momentum and several values of the density. The shaded area is taken from Ref. [40]

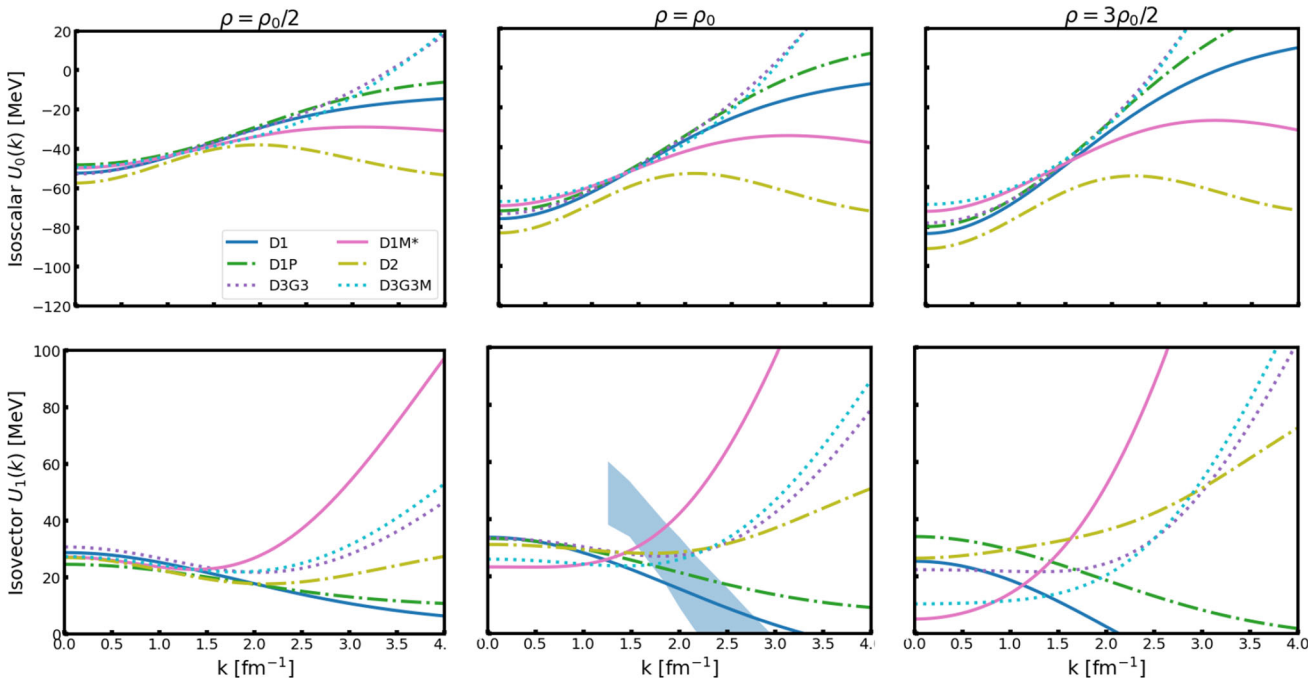

Fig. 7 Same as Fig. 6, but for Gogny interactions

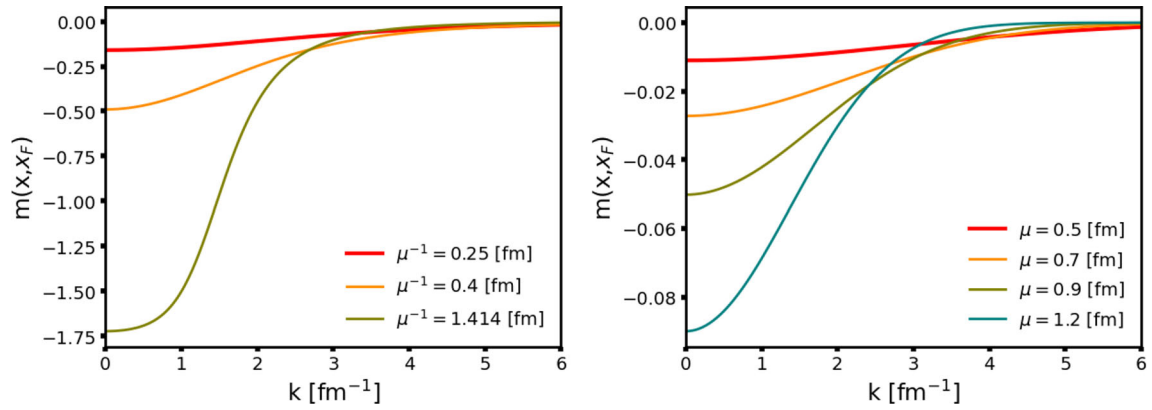

Fig. 8 Functions $\mathrm{m}(x, x_F)$ in SNM at saturation density for several values of μ plotted as a function of momentum. Yukawa (left) and Gaussian (right) form factors

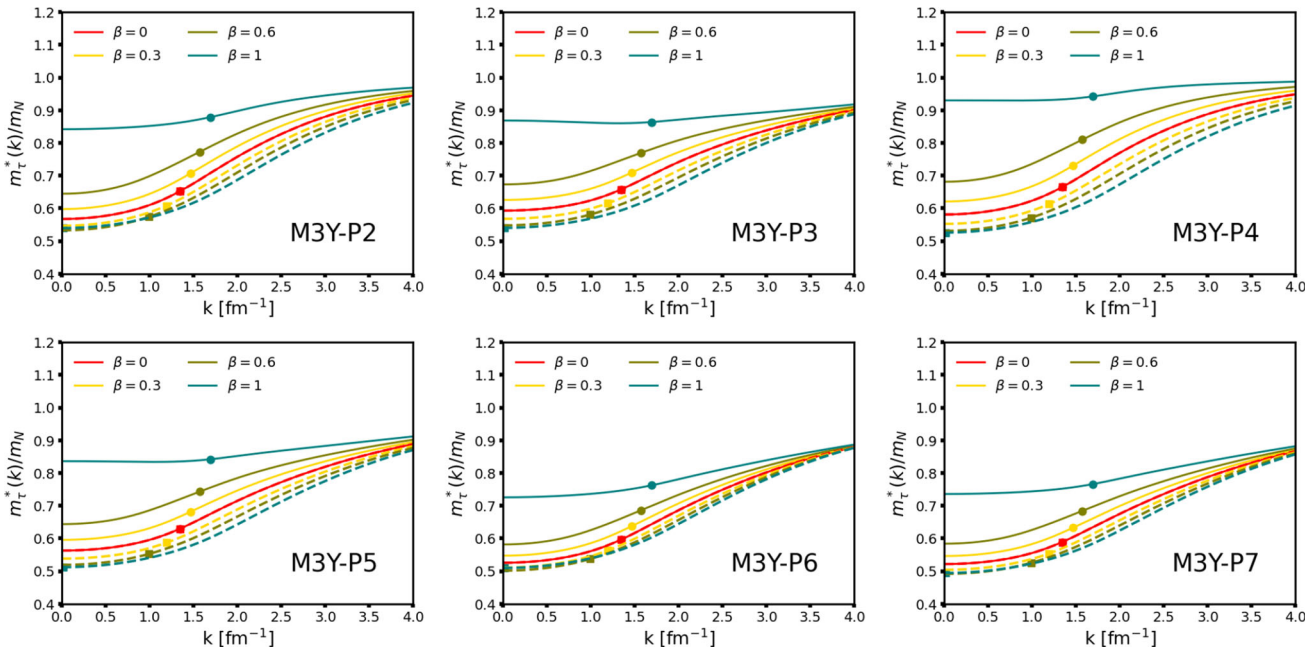

Fig. 9 Effective mass ratio $m^*_\tau(k)/m_N$ for neutrons (solid) and protons (dashed) as a function of the single particle momentum k at saturation density and various isospin asymmetries for Nakada interactions. The symbols denote the effective mass ratio of a neutron (circles) or a proton (square) at the respective Fermi momentum $k_{F\tau}$. See text for details

A more interesting quantity that allows us to summarise the properties of the various interactions is therefore the so-called mass splitting, i.e. the difference between the neutron and proton effective masses at saturation density

$$\begin{aligned}\Delta m(\rho,\beta) &\equiv \frac{m^*_n(\rho,\beta)}{m_N} - \frac{m^*_p(\rho,\beta)}{m_N} \\ &= \left\{1 + \frac{2m}{\hbar^2}\sum_i d_i^2\left[B^i_{nn}\mathrm{m}(x^i_n,x^i_n) + B^i_{np}\mathrm{m}(x^i_n,x^i_p)\right]\right\}^{-1} \\ &- \left\{1 + \frac{2m}{\hbar^2}\sum_i d_i^2\left[B^i_{nn}\mathrm{m}(x^i_p,x^i_p) + B^i_{np}\mathrm{m}(x^i_p,x^i_n)\right]\right\}^{-1}\end{aligned} \tag{21}$$

To obtain this equation, we inject in Eq. 20 $k = k^\tau_F$. For a fixed density, this quantity simply depends on the asymmetry parameter β. Although such a quantity is not strictly speaking an observable, we can still compare with the BHF results [41] and see if the trends are similar or not.

In Fig. 11, we show $\Delta m(\beta)$ calculated at $\rho = 0.16$ [fm^{-3}] as a function of isospin asymmetry for both Gogny and Nakada interactions. As a reference, we report the BHF results discussed in Ref. [41] (shaded band). This band is obtained by taking into account the various changes made in the BHF calculations, such as the variation of the three- and two-body interactions. We see that all Nakada interactions have the correct sign of the mass splitting, although the

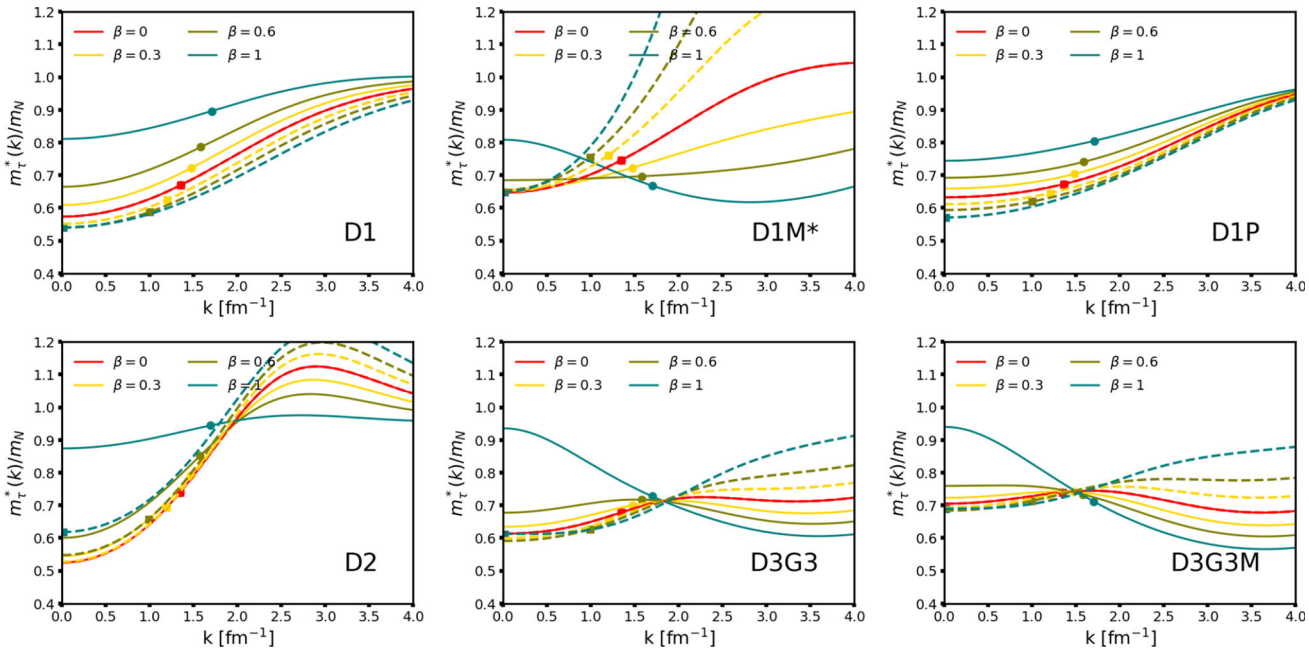

Fig. 10 Same as Fig. 9, but for Gogny interactions

absolute value is slightly overestimated when approaching the PNM limit. However, it remains fairly consistent with the BHF results. The Gogny interactions are also in fairly good agreement with the BHF results, except for D1M* which has an opposite splitting.

Finally, it is interesting to study the evolution of the effective masses of neutrons and protons in function of the density of the system for few selected asymmetries since they can play a role in modelling cold neutron stars [35]. The results are illustrated in Fig. 12 for Nakada and Fig. 13 for Gogny. We notice that all the Nakada interaction have a decreasing monotonous behaviour as we increase the density, while the Gogny show a larger variety of trends: D1 and D1P behaves as the Nakada ones although the asymptotic values of the effective masses are different. The D3G3 and D3G3M present a crossing of the proton and neutron effective mass at around $\rho \approx 0.2$ [fm^{-3}]. Also D1M* and D2 present a crossing, but even more interesting, they do present poles in the proton effective mass in the case of very large isospin asymmetry. This nonphysical feature is also present in some Skyrme functionals and discussed in detail in Ref. [43]. The high density behavior can be compared with some existing *ab-initio* calculations [41], although the results strongly depend on the choice of three-body interaction, we notice that the proton effective mass becomes larger than the neutron one at high density, so a crossing, but with the masses of the two species at first decreasing and then increasing again beyond two times saturation density. Such a feature has not been observed in none of the interactions presented in this article.

3.3 Energy per particle

Having presented the detailed properties of the mean field potential for each interaction, we can now characterise the system by examining its energy per particle. We give here the most general expression as a function of the density and isospin asymmetry

$$\begin{aligned} e_{ANM} &= \frac{E_{\mathrm{ANM}}}{A} \\ &= \frac{3}{10}\frac{\hbar^2}{2m}k_F^2\left[(1+\beta)^{5/3}+(1-\beta)^{5/3}\right] \\ &\quad +\frac{1}{2}(C_0+C_1\beta^2)\rho^{\gamma+1} \\ &\quad +C_{SE}\,\rho^{\gamma_{SE}+1}(3+\beta^2)+C_{TE}\,\rho^{\gamma_{TE}+1}(1-\beta^2) \\ &\quad +\sum_i \frac{1}{2}\rho(A_0^i+A_1^i\beta^2) \\ &\quad +\frac{1}{2}B_{nn}^i\left[\frac{1}{2}(1+\beta)\mathrm{g}(x_n^i)+\frac{1}{2}(1-\beta)\mathrm{g}(x_p^i)\right] \\ &\quad +\frac{1}{2}B_{np}^i\mathrm{h}(x_n^i,x_p^i). \end{aligned} \tag{22}$$

The explicit expression of the functions $\mathrm{g}(x)$ and $\mathrm{h}(x,x')$ is given in Appendix B, and one can see that $\mathrm{g}(x)=\mathrm{h}(x,x)$. These functions contain the form factor contribution resulting from the Fock (exchange) terms. In Ref. [5] such contribution was contained in a function named $\mathcal{W}^F$. In Appendix B is given the relation between both functions for each type of form factor.

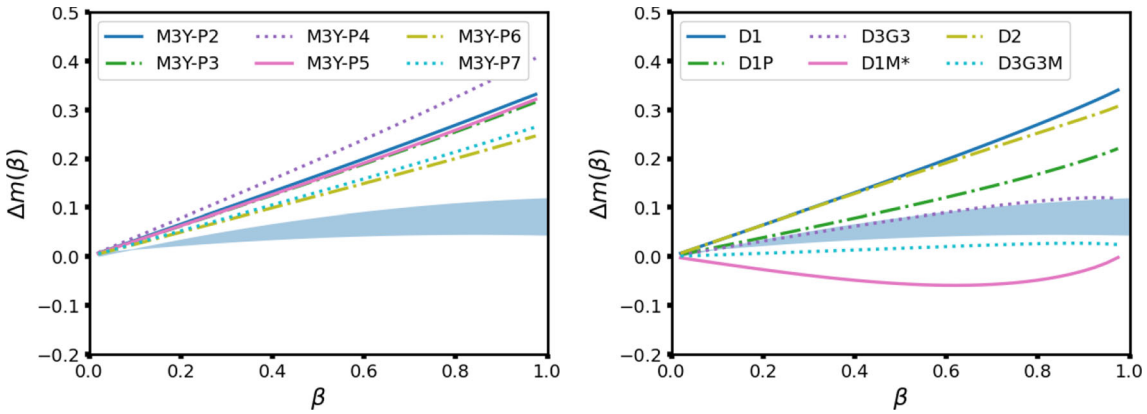

Fig. 11 Difference between the neutron and proton effective mass as defined in Eq. (21) for Nakada (left panel) and Gogny (right panel) at $\rho = 0.16$ fm^{-3} as a function of isospin asymmetry. The band represent the BHF results [41]. See text for details

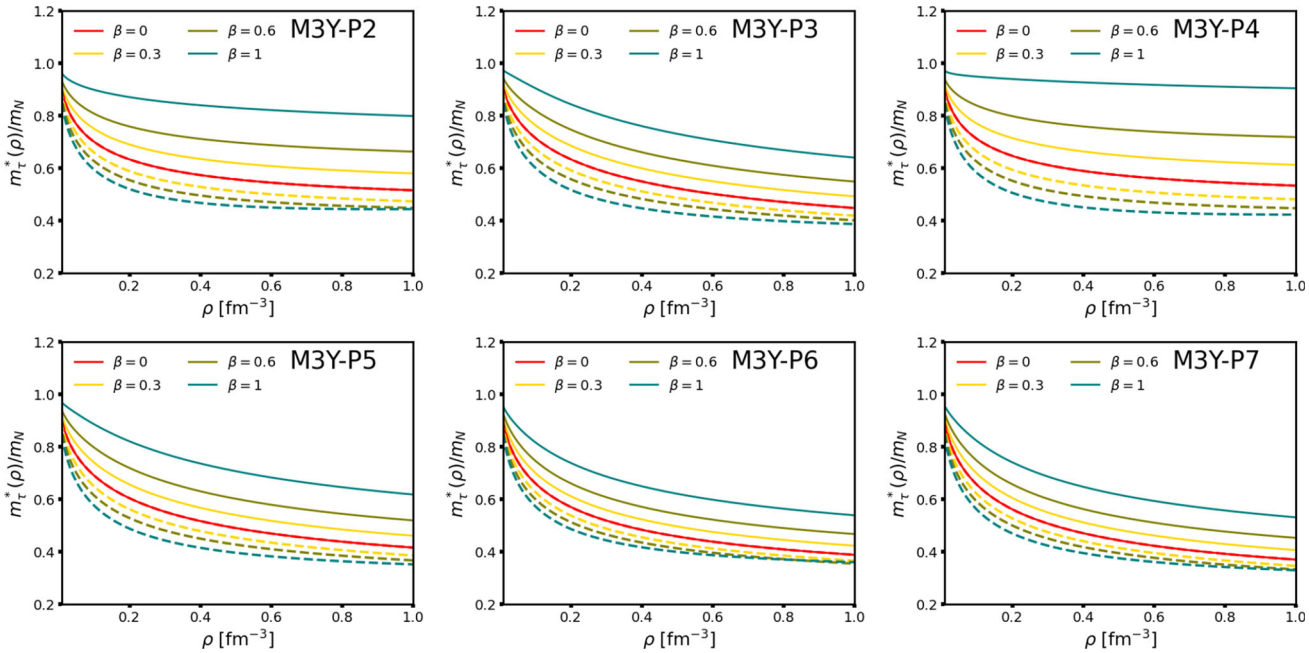

Fig. 12 Effective mass ratio $m^*_\tau(k_F)/m_N$ for neutrons (solid) and protons (dashed) as a function of the density of the system and various isospin asymmetries for Nakada interactions. See text for details

From this equation, depending on the values of β, we can derive some interesting quantities as discussed below.

3.3.1 Symmetric nuclear matter

In case of equal number of neutrons and protons ($\beta = 0$) Eq. (22) becomes

$$e_{SNM} = \left.\frac{E}{A}\right|_{\rm SNM} = \frac{3}{5}\frac{\hbar^2}{2m}k_F^2 + \frac{1}{2}C_0\rho^{\gamma+1} + 3C_{SE}\rho^{\gamma_{SE}+1} + C_{TE}\rho^{\gamma_{TE}+1} + \frac{1}{2}\sum_i\left[A_0^i\rho + B_0^i g(x_F^i)\right]. \quad (23)$$

The equation of state of SNM is quite similar for all the interactions shown in Fig. 14, especially around the saturation density. Given the importance of having good saturation properties to obtain valuable results in atomic nuclei, it is expected that all these interactions have been built with particular care to these quantities (see explicit values in Tables 1-2). In the high-energy region, on the other hand, we observe some variance. For example, at 5 times the saturation density, we observe a maximum difference of ≈ 45 MeV between the different M3Y interactions and of ≈ 40 MeV for the Gogny interactions.

However, in order to assess in a more quantitative way the high density behavior of the equation of state, we will examine other quantities such as the pressure P_{SNM}, the nuclear

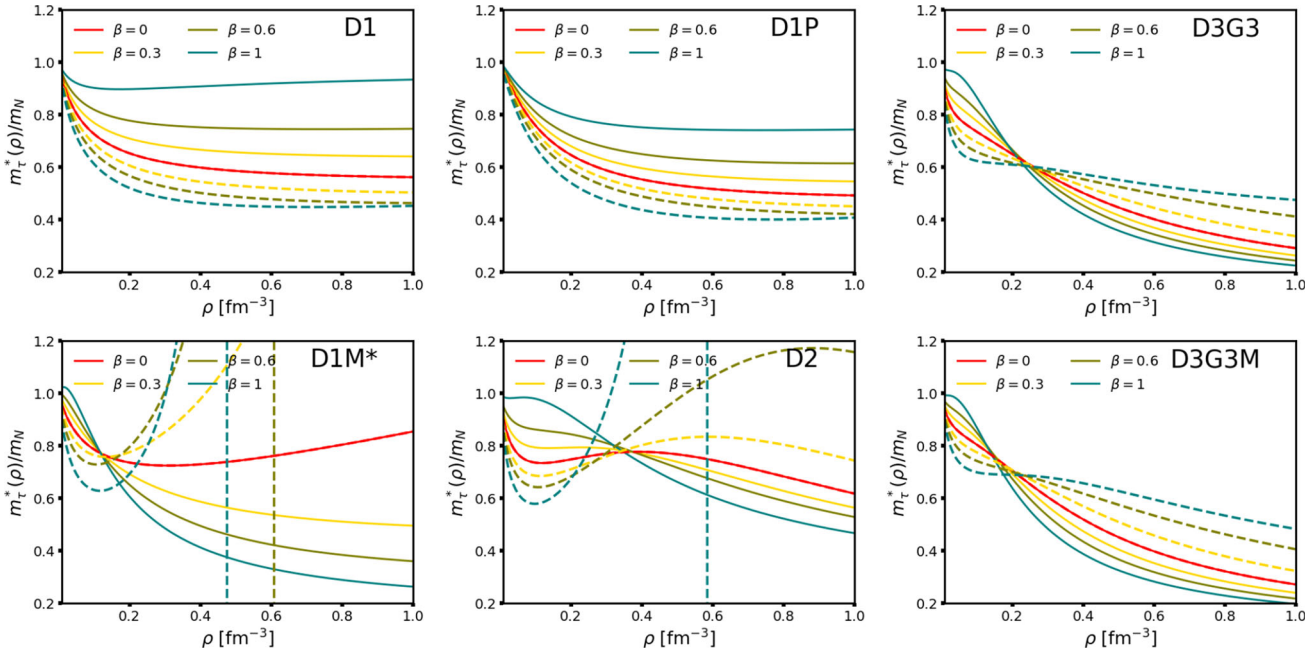

Fig. 13 Same as Fig. 12, but for selected Gogny interactions

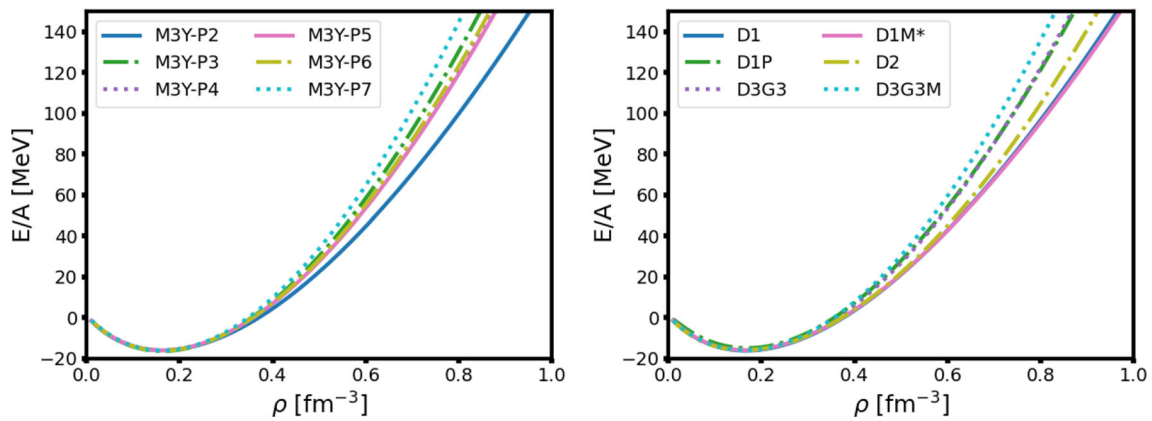

Fig. 14 Energy per particle in SNM as a function of the density of the system for the Nakada (left panel) and Gogny (right panel) interactions. See text for details

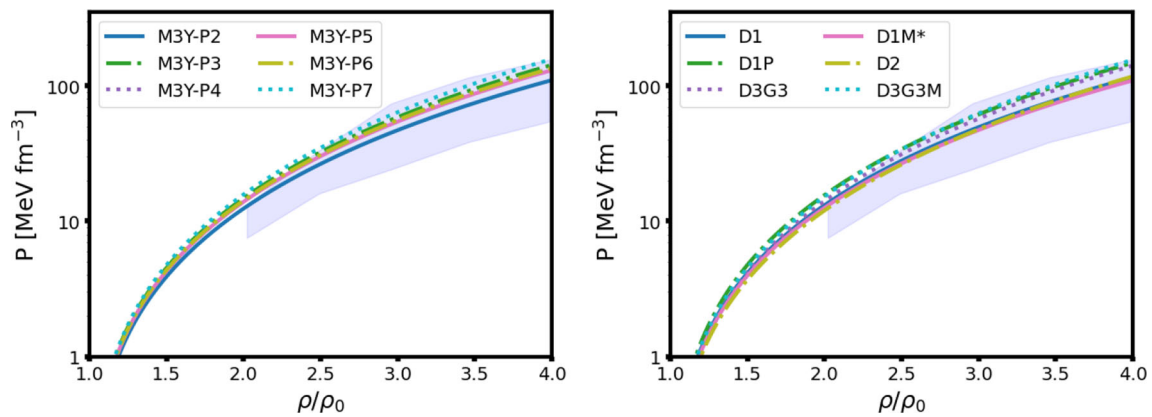

Fig. 15 Pressure in SNM as a function of the density of the system for the Nakada (left panel) and Gogny (right panel) interactions. The density is given in units of the respective saturation density for each interaction. The shaded area is taken from Ref. [44]. See text for details

compressibility K_0 and the skewness Q_0, since in these cases we can compare them with some experimental data. Explicitly, we have

$$\begin{aligned} P_{SNM} &= \rho^2 \frac{\partial e_{SNM}}{\partial \rho} \\ &= \frac{2}{5}\frac{\hbar^2}{2m}\rho k_F^2 + \frac{1}{2}C_0(\gamma+1)\rho^{\gamma+2} \\ &\quad +3(\gamma_{SE}+1)C_{SE}\,\rho^{\gamma_{SE}+2} + (\gamma_{TE}+1)C_{TE}\,\rho^{\gamma_{TE}+2} \\ &\quad + \sum_i \frac{1}{2}A_0^i\rho^2 + B_0^i\,\rho\,\mathrm{p}(x_F^i), \end{aligned} \tag{24}$$

$$\begin{aligned} K_0 &= 9\rho^2 \frac{\partial^2 e_{SNM}}{\partial \rho^2} \\ &= -\frac{6}{5}\frac{\hbar^2}{2m}k_F^2 \\ &\quad +\frac{9}{2}C_0(\gamma+1)\gamma\rho^{\gamma+1} + 27(\gamma_{SE}+1)\gamma_{SE}C_{SE}\,\rho^{\gamma_{SE}+1} \\ &\quad +9(\gamma_{TE}+1)\gamma_{TE}C_{TE}\,\rho^{\gamma_{TE}+1} - 3\sum_i B_0^i\,\mathrm{k}(x_F^i), \end{aligned} \tag{25}$$

$$\begin{aligned} Q_0 &= 27\rho^3 \frac{\partial^2 e_{SNM}}{\partial \rho^3} \\ &= \frac{24}{5}\frac{\hbar^2}{2m}k_F^2 + \frac{27}{2}C_0(\gamma+1)\gamma(\gamma-1)\rho^{\gamma+1} \\ &\quad +81(\gamma_{SE}+1)\gamma_{SE}(\gamma_{SE}-1)C_{SE}\,\rho^{\gamma_{SE}+1} \\ &\quad +27(\gamma_{TE}+1)\gamma_{TE}(\gamma_{TE}-1)C_{TE}\,\rho^{\gamma_{TE}+1} \\ &\quad +3\sum_i B_0^i\,\mathrm{q}(x_F^i). \end{aligned} \tag{26}$$

The explicit expressions of the functions $\mathrm{p}(x)$, $\mathrm{k}(x)$ and $\mathrm{q}(x)$ are given in Appendix B.

From heavy ion collision experiments [44] it is possible to derive a credible range of pressure as a function of density. This is shown in Fig. 15, where the pressure in SNM is plotted for Nakada (left panel) and Gogny (right panel) interactions. We see that all the interactions considered here are inside the shaded area. This is consistent with the relatively small variance in energy per particle observed previously.

The curvature of the equation of state around the saturation density is described by the value of K_0. This quantity is usually related to compressional modes in atomic nuclei [45] as obtained from measurements of giant monopole resonances (GMR) [46]. From Tables 1, 2, we see that the incompressibility values for Gogny range from 209 MeV to 250 MeV, while for Nakada they range from 221 to 255 MeV. Typically the value of $\approx$ 220 MeV is considered acceptable in order to reproduce the GMR in lead isotopes [47]. Instead, a smaller value of $\approx$ 200 MeV is required to reproduce the same quantity in tin isotopes [48]. All interactions presented here are thus compatible with the accepted range of $K_0 \approx 220 \pm 20/30$ MeV proposed in Ref. [35].

Finally, the third derivative of the equation of state is described by Q_0. Typically this value is not constrained in the fitting protocol of the interactions. According to Ref. [35], this quantity should be negative[2] and of the order of magnitude of a few hundreds of MeV. Recently, some new astrophysical models for the nuclear equation of state (EOS) and based on a Taylor series expansion around the saturation density have been proposed for astrophysical applications [49]. Using these models, the authors have been able to infer stronger constraints on Q_0 [50], but how the model assumptions affect these new limits is still a matter of scientific debate. For each interaction, we report the precise value in Tables 1, 2. It is interesting to note that all finite range interactions are consistent with such a weak constraint of Ref. [35].

In Ref. [51] a strong correlation between K_0 and Q_0 is suggested to be due to the density dependent term. We have calculated the Pearson correlation coefficient r [52] and obtained a value of $r = +0.97$ for all Gogny interactions with a *standard* t_3 term (zero range) and two ranges (considering also the Gogny interactions discussed in Ref. [12] and not presented here). However, including the interactions D2, D3G3 and D3G3M, which have a different structure and therefore possibly a different set of correlations, the Pearson coefficient drops to $r = +0.80$, confirming that part of the observed correlation is due to the particular choice of the density dependent term. For the Nakada interaction the correlation is also very strong with $r = +0.97$, showing that using one or two density dependent terms, as long as they are in the zero range, does not change the conclusion.

3.3.2 Pure neutron matter

We now come to the other extreme case of infinite matter without protons, *i.e* the case of pure neutron matter. In this case, the energy per particle is[3]

$$\begin{aligned} e_{PNM} &= \left.\frac{E}{A}\right|_{PNM} = \frac{3}{5}\frac{\hbar^2}{2m}k_{Fn}^2 \\ &\quad +\frac{1}{2}(C_0+C_1)\rho_n^{\gamma+1} + 4C_{SE}\,\rho_n^{\gamma_{SE}+1} \\ &\quad +\frac{1}{2}\sum_i \left[\rho_n(A_0^i + A_1^i) + B_{nn}^i\,\mathrm{g}(x_n^i)\right]. \end{aligned} \tag{27}$$

This quantity is of fundamental importance since it has a direct impact on the structure of compact astrophysical objects [53]. We show the evolution of the energy per particle for the two families of interactions in Fig. 16. As a reference, in the same figure, we show the results obtained with the Chiral Effective field Theory (χEFT) of Ref. [54] at third order (shaded area).

[2] Note that in Ref. [35] the constraint is on K' which is defined as $K' = -Q_0$.

[3] Notice that there is a mistake in Eq. (20) of Ref. [12].

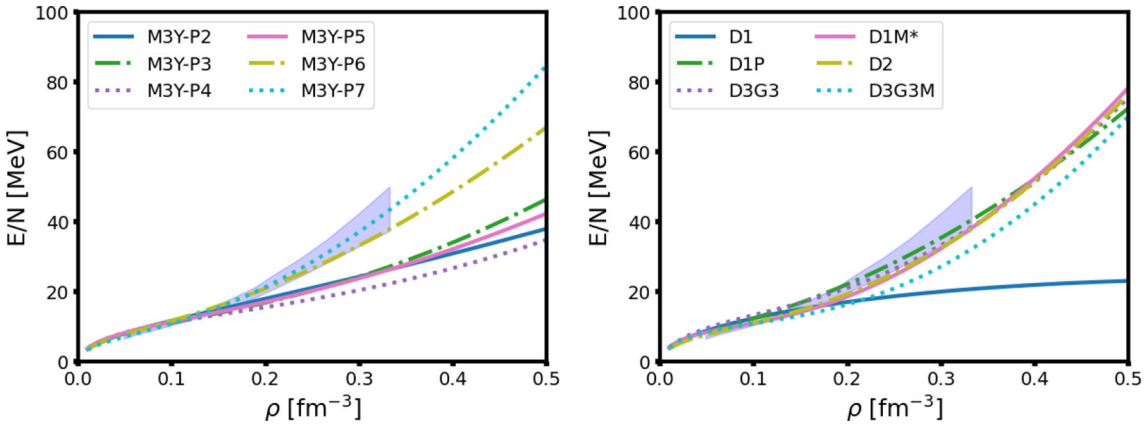

Fig. 16 Energy per particle as a function of the density of the system in PNM for Nakada (left panel) and Gogny (right panel) interactions. The shaded areas represent the results of χEFT obtained in Ref. [54]

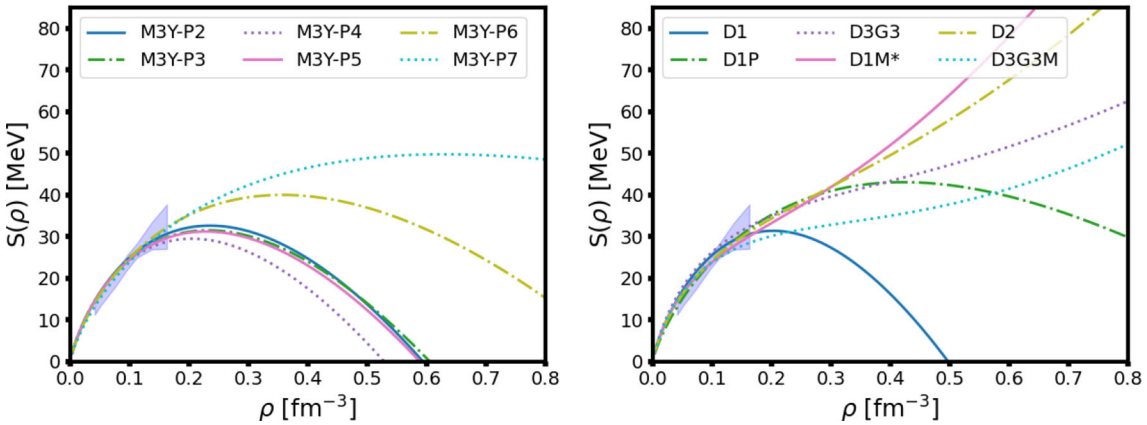

Fig. 17 Symmetry energy as a function of the density of the system for Nakada (left panel) and Gogny (right panel) interactions. The shaded area represent the results of Ref. [60] obtained by analysing IAS in finite nuclei

We note that all Nakada interactions lead to a non-collapsing EOS (such as in the case of the Gogny D1 interaction), but are not compatible with the χEFT constraints, except for the most recent M3Y-P6 and M3Y-P7. This is also usually the case for the first versions of the Gogny interaction as shown in Ref. [12], but the most recent parameterisations tend to provide quite stiff PNM EOS in fair agreement with recent *ab-initio* results.

The high density behavior of the EOS is not fully constrained by these *ab-initio* calculations, but it can be inferred by combining our knowledge of neutron stars [55,56]. For this purpose, it is useful to provide the expression of the pressure of PNM as

$$\begin{aligned} P_{PNM} = & \frac{2}{5}\frac{\hbar^2}{2m}k_{Fn}^2\rho_n + \frac{1}{2}(C_0+C_1)(\gamma+1)\rho_n^{\gamma+2} \\ & +4C_{SE}\,(\gamma_{SE}+1)\rho_n^{\gamma_{SE}+2} \\ & +\sum_i \frac{1}{2}(A_0^i+A_1^i)\rho_n^2 + B_{nn}^i\rho_n\,\mathrm{p}(x_n^i). \end{aligned} \tag{28}$$

This quantity is used to solve the relativistic Tolman-Oppenheimer-Volkov (TOV) [57] equations as discussed in Sect. 3.5.

3.4 Isovector properties

In the previous sections, we have studied various properties of the infinite medium for a fixed isospin asymmetry. We now examine its isovector properties. To do this, we consider the symmetry energy $S(\rho)$ which is obtained as the second derivative of the energy per particle with respect to the isospin asymmetry parameter

$$\begin{aligned} S(\rho) = & \frac{1}{2}\frac{\partial^2 e_{ANM}(\rho,\beta)}{\partial\beta^2}\bigg|_{\beta=0} \\ = & \frac{1}{3}\frac{\hbar^2}{2m}k_F^2 + \frac{1}{2}C_1\rho^{\gamma+1} + C_{SE}\,\rho^{\gamma_{SE}+1} - C_{TE}\,\rho^{\gamma_{TE}+1} \\ & +\sum_i \frac{1}{2}A_1^i\rho + \frac{1}{6}\left[B_{nn}^i\mathrm{s}_1(x^i) + B_{np}^i\mathrm{s}_2(x^i)\right]. \end{aligned} \tag{29}$$

In Fig. 17 we show the behavior of $S(\rho)$ as a function of density for the different interactions considered here. All interactions are within a narrow energy window around the saturation density. We report the precise value at the saturation density in Tables 1, 2, mainly because there are some stringent constraints coming from previous studies of nuclear masses and neutron stars [35,58], but, as one moves to higher densities, we observe a wide variety of trends. Some interactions, such as D1 and M3Y-P(2-5), give negative values, implying a crossing between the EOS in SNM and PNM. Such a crossing is most likely non-physical, since the corresponding hadronic equation of state would not be able to support very massive neutron stars. A very detailed analysis done in Ref. [59] show that effective interactions leading to very soft or even negative $S(\rho)$ at suprasaturation densities in neutron are not capable to produce hadronic equation of state capable of sustaining neutron stars heavier than two times the Solar mass. On the other hand, its effect on finite nuclei is not entirely clear, since in all cases it occurs at densities well above saturation. On these figures we also report as a shaded area the constraints obtained in Ref. [60] using excitation energies of isobaric analog states (IAS) in atomic nuclei. We see that essentially all interactions do respect such a constraint.

Another interesting quantity used to determine the properties of the interaction is the slope of the symmetry energy

$$\begin{aligned} L(\rho) &= 3\rho\frac{\partial S(\rho)}{\partial\rho} \\ &= +\frac{2}{3}\frac{\hbar^2}{2m}k_F^2 + \frac{3}{2}(\gamma+1)C_1\rho^{\gamma+1} \\ &\quad +3(\gamma_{SE}+1)C_{SE}\rho^{\gamma_{SE}+1} - 3(\gamma_{TE}+1)C_{TE}\rho^{\gamma_{TE}+1} \\ &\quad +\sum_i \frac{3}{2}A_1^i\rho + \frac{1}{6}\left[B_{nn}^i \mathrm{l}_1(x^i) + B_{np}^i \mathrm{l}_2(x^i)\right]. \end{aligned} \tag{30}$$

A strong correlation has been found between $L(\rho_0)$ and the neutron skin of heavy nuclei [61]. By combining the results of 24 different analyses, the authors of Ref. [62] give a value of $L(\rho_0) = 58 \pm 19$ MeV with 68% confidence. This means that all finite-range interactions except D1P, D2, M3Y-P6 and M3Y-P7 give a result that is in tension with the current knowledge of such a quantity. Recent studies based on the results of the PREX II experiment [63] even suggest a value of $L(\rho_0) = 106 \pm 37$ MeV [64] which is much higher than the previous estimate. Such a result is clearly incompatible with all the finite range models analysed here and in Ref. [12]. To date, the scientific debate on these conclusions is still open, but it is clear that the finite range interactions tend to underestimate this quantity and thus, according to the correlation detected in Ref. [61], are most likely not suitable to describe the appearance of a large neutron skin in heavy nuclei. Some additional studies are needed to clarify this point. However, if the high value of L_0 is confirmed, it would represent a major challenge in the finite-range interaction optimisation procedure and would probably require some modifications to the structure of the central term.

As in the isoscalar case, we can also consider the higher order derivatives of the symmetry energy such as

$$\begin{aligned} K_{\rm sym} &= 9\rho^2\frac{\partial^2 S(\rho)}{\partial\rho^2} \\ &= -\frac{2}{3}\frac{\hbar^2}{2m}k_F^2 + \frac{9}{2}(\gamma+1)\gamma C_1\rho^{\gamma+1} \\ &\quad +9(\gamma_{SE}+1)\gamma_{SE}C_{SE}\,\rho^{\gamma_{SE}+1} \\ &\quad -9(\gamma_{TE}+1)\gamma_{TE}C_{TE}\,\rho^{\gamma_{TE}+1} \\ &\quad -\frac{2}{3}\sum_i\left[B_{nn}^i \mathrm{k}_1(x^i) + B_{np}^i \mathrm{k}_2(x^i)\right], \end{aligned} \tag{31}$$

$$\begin{aligned} Q_{\rm sym} &= 27\rho^3\frac{\partial^3 S(\rho)}{\partial\rho^3} \\ &= \frac{8}{3}\frac{\hbar^2}{2m}k_F^2 + \frac{27}{2}(\gamma+1)\gamma(\gamma-1)C_1\rho^{\gamma+1} \\ &\quad +27(\gamma_{SE}+1)\gamma_{SE}(\gamma_{SE}-1)C_{SE}\,\rho^{\gamma_{SE}+1} \\ &\quad -27(\gamma_{TE}+1)\gamma_{TE}(\gamma_{TE}-1)C_{TE}\rho^{\gamma_{TE}+1} \\ &\quad +\frac{1}{3}\sum_i\left[B_{nn}^i \mathrm{q}_1(x^i) + B_{np}^i \mathrm{q}_2(x^i)\right]. \end{aligned} \tag{32}$$

In this case we do not have precise constraints against which to compare our results. According to the authors of Refs. [50,65], one can infer some values of Q_{sym} by exploiting its correlation with $3S(\rho_0) - L(\rho_0)$. For the Nakada interactions we observed a Pearson coefficient of $r = -0.99$, while for all available Gogny interactions (including the one in Ref. [12]) we have $r = -0.78$. The large variation in the r coefficient may be a sign of a limitation of the model itself rather than a true correlation, as discussed in Ref. [66] for the t_3 versus α correlation in the case of Skyrme interactions.

3.5 Neutron stars

In this section, we present the basic features of a non-accreting neutron star (NS) at zero temperature, using the finite-range interactions discussed in the text. In our description, we assume that the composition of the star consists only of neutrons, protons and electrons in β equilibrium [57]. Also assuming charge neutrality, it follows that the proton density is equal to the electron density. As discussed in Ref. [67], the β equilibrium condition within the parabolic approximation leads to the relation

$$\mu_e = \mu_n - \mu_p \approx 4(1-2Y_p)S(\rho), \tag{33}$$

where $\mu_{e,n,p}$ are the chemical potentials of the different species. Higher order terms of the symmetry energy do contribute to this equation as discussed in Ref. [68], so that one should take them into account in order to get accurate

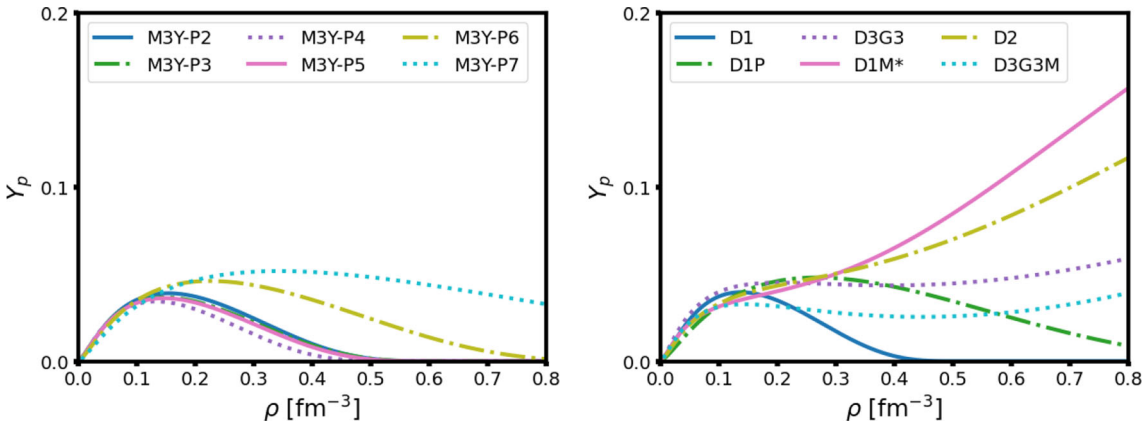

Fig. 18 Proton fraction Y_p as a function of the density of the star for Nakada (left panel) and Gogny (right panel) interactions

results. By solving this equation, under the assumption of ultra-relativistic electrons, we obtain the evolution of the proton fraction Y_p at various densities. In Fig. 18, we show the evolution of Y_p as a function of the density of the system for the Nakada (left panel) and the Gogny (right panel) interactions.

Since essentially all interactions give very close values of $S(\rho)$ around the saturation density, we observe that they all lead to essentially the same value of Y_p according to Eq. 33. On the contrary, in the high density region we observe a large variety of results. All Nakada interactions except M3Y-P7 lead to a full neutronisation of the system. This is also the case for the D1 and D1P Gogny interactions. The interest of Y_p is related to the possibility of allowing or not the direct Urca process during the cooling of a NS [69]. This can take place when $Y_p \approx 0.11 - 0.15$ [70]. We see that only two Gogny interactions satisfy such a criterion, namely D2 and D1M* (albeit at very high densities). By studying the thermal evolution of a NS [71], it would then be possible to provide some information on this quantity and indirectly on the symmetry energy at high density [72]. Using the previous results, we can thus calculate the hadronic equation of state, which will be used to describe some macroscopic properties of the NS. To do this, we solve the TOV equations [57]

$$\frac{dP(r)}{dr} = -\frac{Gm(r)\varepsilon(r)}{r^2}\left[\left(1+\frac{P(r)\varepsilon(r)}{c^2}\right)\left(1+\frac{4\pi r^3 P(r)}{\varepsilon(r)c^2}\right)\right]\left[\left(1-\frac{2Gm(r)}{rc^2}\right)\right]^{-1}, \tag{34}$$

$$\frac{dm(r)}{dr} = 4\pi r^2 \varepsilon(r). \tag{35}$$

G is the gravitational constant and $\varepsilon(r)$ is the total energy density of the system, thus including also the electron contribution. See Ref. [68] for more details on the electronic contribution.

In the crust region of the star, we have crystalline structures which cannot be described using a INM approximation. We therefore use the results of Ref. [73] to describe the NS at densities lower than $\rho \approx 0.08$ fm^{-3}. This small inconsistency will not affect the results concerning the radius or the maximum mass of a NS by more than 5% [74]. In Fig. 19, we show the mass-radius relation obtained by solving the TOV equations. The interactions with a collapsing EOS in PNM such as D1 do not produce any physical solution once injected into the TOV equations.

Most of the finite range interactions are incompatible with current constraints on the maximum NS mass as given in Ref. [75]. We also refer to the discussion in Ref. [12]. Only D1M*, D2,D3G3, D3G3M and M3Y-P7 provide a NS with a mass greater than 2 solar masses. Recent measurements reported in Ref. [76] give a maximum mass of 2.35 $M_\odot$. This constraint, if confirmed, would rule out all finite range interactions except D3G3M, which is marginally compatible with these new data. Considering only those interactions that satisfy the 2 solar masses constraint, we find that the radii at 1.4 $M_\odot$ are about $\approx$ 11 km. This value is in good agreement with recent constraints from gravitational wave studies [77].

4 Pairing in infinite matter

In the previous analysis, we have considered the system only at the HF level. It is now interesting to study its superfluid properties using the various interactions described in the present article. As discussed in the literature, we can describe a non-polarised infinite system by means of simple BCS equations [78–80]. They read

$$\Delta_{\alpha\alpha'}(\mathbf{k}) = -\sum_{\beta\beta'\mathbf{k}'} \frac{\langle \mathbf{k}\alpha\alpha'|v|\mathbf{k}'\beta\beta'\rangle \Delta_{\beta\beta'}(\mathbf{k}')}{2\sqrt{(\varepsilon_k-\varepsilon_F)^2+\frac{1}{2}\mathrm{Tr}[\Delta\Delta^\dagger](\mathbf{k}')}}, \tag{36}$$

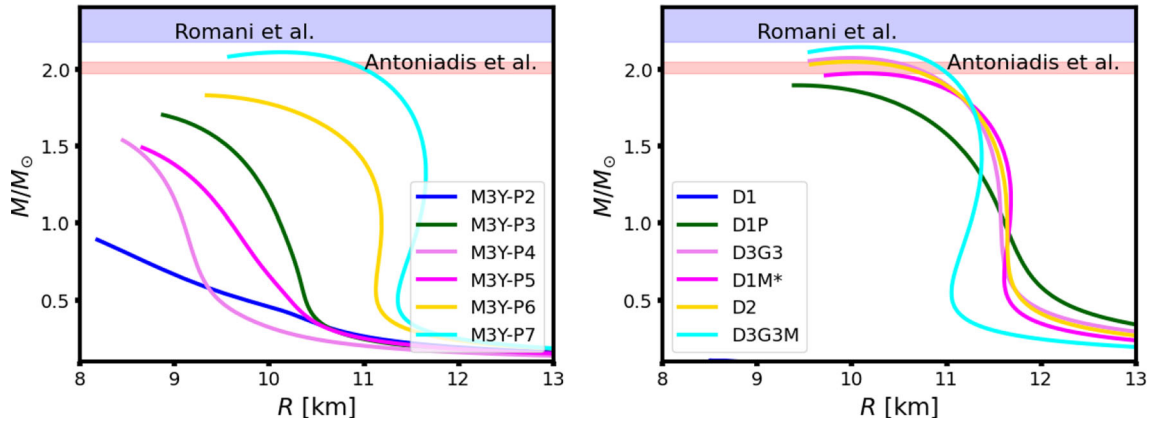

Fig. 19 Mass-radius relation for NS obtained from the EoS by solving TOV equations for selected Nakada (left panel) and Gogny (right panel) interactions. The two horizontal bands refer to the NS mass measurements of Antoniadis et al. $M/M_{Sun} = 2.01 \pm 0.04$ [75] and Romani et al. $M/M_{Sun} = 2.35 \pm 0.17$ [76]. See text for details

where $\langle \mathbf{k}\alpha\alpha'|v|\mathbf{k}'\beta\beta'\rangle$ is the antisymmetrized matrix element of the effective pairing interaction in momentum space. $\varepsilon_k = \frac{\hbar^2 k^2}{2m} + U(k)$ is the single particle spectrum, ε_F the Fermi energy, α, β indices stand for the single-particle spin states and $\mathbf{k}(\mathbf{k}')$ their momenta. For simplicity we have omitted the isospin index, since we only consider Cooper pairs of the same species. The pairing gap is therefore a 2×2 matrix in single-particle spin space.

The basis function of the system are plane waves, which we can couple in order to work with a good total spin S and relative angular momentum L. If J is the total angular momentum, we can distinguish the different couplings using the spectroscopic notation $^{2S+1}L_J$.

The $^1S_0$ coupling is the most important for providing a good description of the pairing properties of atomic nuclei [81]. Other channels may also play a role in astrophysical scenarios, such as the cooling of neutron stars [71], but they are not considered here. A number of studies based on bare NN interactions have shown that the $^1S_0$ pairing gap in infinite matter calculated at the BCS level is not strongly dependent on the choice of interaction [82], thus providing some guidance on how to construct effective interactions. In the other channels the situation is less clear [80] and the results show a much stronger dependence on the details of the interaction. The situation becomes even more complicated when considers many body effects beyond BCS [83,84].

In the spin singlet channel $^1S_0$, the BCS equations reduce to [85]

$$\Delta(k) = -\frac{1}{2}\int_0^\infty dk' k'^2 \frac{v(k,k')\Delta(k')}{\sqrt{(\varepsilon_k - \varepsilon_F)^2 + \Delta(k')^2}}. \tag{37}$$

The Nakada pairing matrix elements reads

$$v(k,k') = \frac{1}{\pi}\sum_i \frac{t_i^{SE}}{2kk'\mu_i} \log\left[\frac{4kk'}{(k-k')^2+\mu_i^2} + 1\right] + \frac{1}{2\pi^2} t_\rho^{SE} \rho^{\gamma_{SE}}, \tag{38}$$

while for Gogny interactions we have [85]

$$v(k,k') = \frac{1}{\pi^{1/2} kk'} \sum_i C_i \exp\left[-\frac{\mu_i^2}{4}(k^2 + k'^2)\right] \sinh\left(\frac{\mu_i^2 kk'}{2}\right) + \frac{1}{2\pi^2}\sum_j t_{0j}(1 - x_{0j})\rho^{\gamma_j}, \tag{39}$$

where $C_i = \mu_i(W_i - B_i - H_i + M_i)$.

Note that for most Gogny interactions $x_0 = 1$, so the density-dependent term does not enter the pairing matrix elements and there is no divergence due to the presence of a Dirac delta in the matrix element [6]. In some interactions such as D1P $x_0 \neq 1$. As a consequence, a cut-off in quasi-particle space is required to make the calculations converge [86]. For D1P, the authors fix the value of the integral of the pairing gap in infinite matter to the same value as for D1, so the cut-off is adjusted to satisfy this constraint. However, we have found that the contribution of the density dependent terms to D1P is rather weak, so there is actually no need to fine-tune the cut-off.

In Fig. 20 we show the evolution of the pairing gap at the Fermi momentum as a function of k_F in SNM for our two families of interactions: Nakada (left panel) and Gogny (right panel). On the same figure we also plot the results obtained from *ab initio* calculations suggested in Ref. [85]. These calculations are based on a $V_{\text{low-k}}$ interaction at BCS level on top of a renormalised single particle spectrum computed using Brueckner Hartree Fock methods. We conclude that at the BCS level the pairing gap should have a maximum around $k_F \approx 0.8$ fm^{-1} at about $\Delta_{k_F} \approx 2.5 - 3$ MeV. We observe that M3Y-P3, P4 and P5 follow such a behavior,

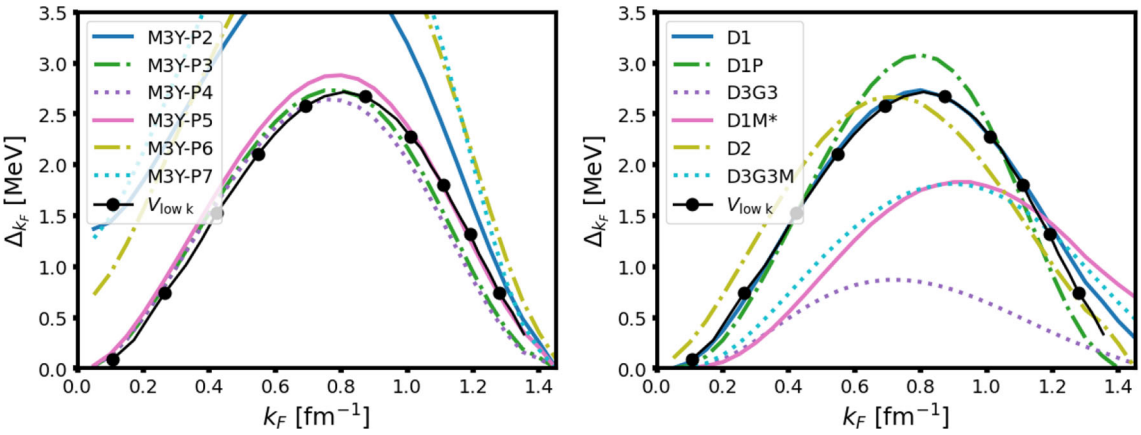

Fig. 20 Evolution of the pairing gap at k_F in SNM as a function of the Fermi momentum k_F for Nakada (left panel) and Gogny (right panel) interactions. We also report on the figure (circles) the results obtained in Ref. [85] based on $V_{\text{low-k}}$ interaction at BCS level. See text for details

while M3Y-P2, P6, P7 lead to a very strong pairing gap. It is worth noting that, as discussed in Ref. [22], the convergence in momentum space of the BCS equations using the Nakada interaction is extremely slow and requires the inclusion of states beyond $k = 10$ fm^{-1}, leading to a too large basis set to treat atomic nuclei. As a consequence, Nakada introduced a cut-off also in the finite range part, as presented in Ref. [22], where different types of cut-offs are discussed. For the sake of simplicity we have simply implemented the sharp cut-off at $k_c = 4$ fm^{-1} for all interactions. This is somehow arbitrary, but we have not been able to find more details about the basis size of the most recent interactions such as P6 and P7. Most likely a smaller space is used. If we use $k_c = 1.55$ fm^{-1} (which corresponds roughly to the basis used for finite nuclei [87]) we obtain a maximum value of the pairing gap in SNM of $\Delta_{k_F} = 3.3$ MeV for M3Y-P6 and $\Delta_{k_F} = 3.8$ MeV for M3Y-P7, which are now closer to the *ab-initio* BCS results. We conclude that since these interactions have been carefully tuned to reproduce the pairing properties within the chosen pairing window, as a consequence one needs its exact definition in order to reproduce the results correctly. Therefore, apart from M3Y-P5, for which an explicit calculation is provided, we cannot draw any conclusions about the other interactions.

Contrary to the Nakada case, the Gogny interactions do not have a pairing window (apart from D1P as discussed above). Leaving aside D3G3, which is unable to produce a sufficiently strong pairing gap, we can identify two types of structure: D1, D1P and D2, all of which give a pairing curve with a maximum around $k_F \approx 0.8$ fm^{-1} with a gap of $\Delta_{k_F} \approx 3$ MeV; D1M* and D3G3M with a maximum value of the gap at only 2 MeV, but the shape of the curve is shifted at high densities so that the maximum occurs at $k_F \approx 1$ fm^{-1}. The region of interest for pairing in atomic nuclei is around $k_F \approx 1.2 - 1.3$ fm^{-1}. In this interval, all Gogny interactions still produce a pairing gap of about $1-1.5$ MeV, which is compatible with the typical value of the gap in a heavy nucleus [78]. This is not the case for D3G3, and as discussed in Ref. [33], the resulting pairing gap in finite nuclei is too weak compared to experimental ones.

5 Conclusions

In this article we have carried out a systematic investigation of the isovector properties of the Nakada finite range interactions. Following the scheme proposed in Ref. [12], we have studied all relevant quantities that characterise infinite systems at the Hartree-Fock level, such as the single particle potential, the effective mass, the equation of state and the pressure. We have also included the case of superfluid systems relevant to the study of atomic nuclei. We have compared the Nakada results with those obtained with the latest Gogny parameterisations not discussed in Ref. [12]. These new interactions, in particular D2, required the introduction of additional terms in the various equations, and we have therefore presented all these necessary modifications in detail in the Appendix.

One of the main conclusions is that the Gogny interactions typically show quite a large variance in results compared to the Nakada interactions. In the case of Gogny, especially for the most recent ones, the fitting protocols vary a lot, although they have some common features. Such a large variance is very interesting as it allows to explore a very large parameter space and thus to infer the quality of the structure of the interaction itself and to identify possible constraints.

In general, the conclusions presented in Ref. [12] regarding the predicted quantities of the various interactions in the isovector channels still hold here: a lack of direct constraint can lead to a variety of behaviours, as in the case of the high-momentum sector of the single-particle potential. However, future parameterisations should benefit from new

results. Thanks to advances in astrophysical observations, it is becoming increasingly common to integrate astrophysical data into the fitting protocol. For example, we can see the evolution of the EOS in PNM, from very soft ones such as D1 or M3Y-P2 to the latest parameterisations, which give a very stiff EOS capable of supporting the heaviest NS observed so far. *Ab-initio* methods have also made great progress, so that we now have access to a variety of results with more controlled extrapolations and also credible regions that can be used within a fitting protocol to improve the isovector properties of the effective interactions.

We conclude by noting that the finite-range interactions have historically had some problems in satisfying the accepted constraints of infinite matter. Therefore, they were not adapted to perform astrophysical calculations. Today this is no longer the case, and one can obtain very accurate Nakada or Gogny interactions, which are able to reproduce the properties of atomic nuclei and infinite matter equally well. Some open questions, such as the small values of the slope of the symmetry energy, will probably require a better exploration of the parameter space or even a change in the analytical forms of the interactions.

Acknowledgements We thank A. Rios for useful discussions.

Data Availability Statement This manuscript has no associated data. [Author's comment: The parameters of the D3G3M interaction can be provided on request.]

Code Availability Statement This manuscript has no associated code/software. [Author's comment: This article is a purely theoretical study and does not involve code or software.]

Appendix A Gogny's coupling constants

For completeness, we collect here the combinations of parameters A, B, C, which were defined in Ref. [12]. The general form of a Gogny interaction, restricted to its central and density-dependent terms is written as

$$V_{\text{Gogny}}(r) = \sum_j t_0^j (1 + x_0^j P_\sigma)\rho^{\gamma_j}\delta(r) + \sum_i (W_i + B_i P_\sigma - H_i P_\tau - M_i P_\sigma P_\tau)\mathrm{e}^{-r^2/\mu_i^2}. \tag{A1}$$

The form given here is general to accommodate additional density dependencies such as in D1P. The special case of Gogny D2 is discussed in detail in Appendix C.

$$A_0^i = \frac{\pi^{3/2}\mu_i^3}{4}(4W_i + 2B_i - 2H_i - M_i) \tag{A2}$$

$$A_1^i = \frac{\pi^{3/2}\mu_i^3}{4}(-2H_i - M_i) \tag{A3}$$

$$B_{nn}^i = -\frac{1}{\sqrt{\pi}}(W_i + 2B_i - H_i - 2M_i) \tag{A4}$$

$$B_{np}^i = \frac{1}{\sqrt{\pi}}(H_i + 2M_i) \tag{A5}$$

$$C_0^j = \frac{3}{4}t_0^j \tag{A6}$$

$$C_1^j = -\frac{1}{4}t_0^j(1 + 2x_0^j) \tag{A7}$$

$$C_{SE} = 0 \tag{A8}$$

$$C_{TE} = 0 \tag{A9}$$

$$B_{nn}^d = -\frac{1}{\mu_d^3\pi^2}(W_d + 2B_d - H_d - 2M_d) \tag{A10}$$

$$B_{np}^d = \frac{1}{\mu_d^3\pi^2}(H_d + 2M_d) \tag{A11}$$

Appendix B Momentum-dependent functions

We provide here the explicit expressions of the various momentum-dependent functions entering the expressions given in this article.

B.1 Nakada

We define some special functions in terms of dimensionless variables $z = k/\mu$. The subindex F refers to the Fermi momentum k_F.

$$\mathrm{g}(z) = 12z - \frac{2}{z} - 16\mathrm{ArcTan}(2z) + \left(\frac{6}{z} + \frac{1}{2z^3}\right)\mathrm{Log}(1 + 4z^2) \tag{B1}$$

$$\mathrm{h}(z_1, z_2) = \frac{4z_1z_2\{3(z_1^2 + z_2^2) - 1\}}{z_1^3 + z_2^3} - 16\mathrm{ArcTan}(z_1 + z_2) + 16\frac{z_2^3 - z_1^3}{z_1^3 + z_2^3}\mathrm{ArcTan}(z_2 - z_1) - \frac{3(z_2^2 - z_1^2)^2 - 6(z_1^2 + z_2^2) - 1}{z_1^3 + z_2^3} \times \mathrm{Log}\frac{1 + (z_1 + z_2)^2}{1 + (z_1 - z_2)^2} \tag{B2}$$

The latter function is related to the $\mathcal{W}^F$ function defined in Ref. [5] as

$$\mathcal{W}^F(k_1,k_2)=\frac{2\pi^3}{3}(k_1^3+k_2^3)\mathrm{h}(z_1,z_2) \tag{B3}$$

The other functions read

$$\begin{aligned}\mathrm{u}(z,z_F)=8z_F+2\frac{-z^2+z_F^2+1}{z}\mathrm{Log}\frac{(z_F+z)^2+1}{(z_F-z)^2+1}\\ -8\mathrm{Arctan}\,(z_F+z)-8\mathrm{Arctan}\,(z_F-z)\end{aligned} \tag{B4}$$

$$\mathrm{u}_1(z,z_F)=\frac{4z_F^2}{z}\,\mathrm{Log}\frac{(z_F+z)^2+1}{(z_F-z)^2+1} \tag{B5}$$

$$\mathrm{m}(z,z_F)=4\frac{z_F}{z^2}-\frac{z_F^2+z^2+1}{z^3}\mathrm{Log}\frac{1+(z_F+z)^2}{1+(z_F-z)^2} \tag{B6}$$

$$\mathrm{p}(z)=\frac{1}{z}+2z-\left(\frac{1}{z}+\frac{1}{4z^3}\right)\mathrm{Log}(1+4z^2) \tag{B7}$$

$$\mathrm{k}(z)=\frac{6}{z}+4z-\left(\frac{3}{2z^3}+\frac{4}{z}\right)\mathrm{Log}(1+4z^2) \tag{B8}$$

$$\begin{aligned}\mathrm{q}(z)=20z+\frac{54}{z}-\frac{16z}{1+4z^2}\\ -\left(\frac{27}{2z^3}+\frac{28}{z}\right)\mathrm{Log}(1+4z^2)\end{aligned} \tag{B9}$$

$$\mathrm{s}_1(z)=8z-\frac{2}{z}\,\mathrm{Log}(1+4z^2) \tag{B10}$$

$$\mathrm{s}_2(z)=8z-\left(8z+\frac{2}{z}\right)\mathrm{Log}(1+4z^2) \tag{B11}$$

$$\mathrm{l}_1(z)=8z-\frac{16z}{4z^2+1}+\frac{2}{z}\mathrm{Log}(1+4z^2) \tag{B12}$$

$$\mathrm{l}_2(z)=-8z-\left(8z-\frac{2}{z}\right)\mathrm{Log}(1+4z^2) \tag{B13}$$

$$\begin{aligned}\mathrm{k}_1(z)=4z-\frac{32z^3}{(4z^2+1)^2}\\ -\frac{12z}{4z^2+1}+\frac{2}{z}\mathrm{Log}(1+4z^2)\end{aligned} \tag{B14}$$

$$\mathrm{k}_2(z)=-\frac{8z}{4z^2+1}-\left(4z-\frac{2}{z}\right)\mathrm{Log}(1+4z^2) \tag{B15}$$

$$\begin{aligned}\mathrm{q}_1(z)=40z-\frac{1024z^5}{(4z^2+1)^3}-\frac{384z^3}{(4z^2+1)^2}\\ -\frac{152z}{4z^2+1}+\frac{28}{z}\mathrm{Log}(1+4z^2)\end{aligned} \tag{B16}$$

$$\begin{aligned}\mathrm{q}_2(z)=16z-\frac{128z^3}{(4z^2+1)^2}-\frac{128z}{4z^2+1}\\ -\left(40z-\frac{28}{z}\right)\mathrm{Log}(1+4z^2)\end{aligned} \tag{B17}$$

B.2 Gogny

We define some special functions in terms of dimensionless variables $z=k\mu$. The subindex F refers to the Fermi momentum k_F. We have

$$\begin{aligned}\mathrm{g}(z)=\frac{2}{z^3}-\frac{3}{z}-\left(\frac{2}{z^3}-\frac{1}{z}\right)\mathrm{e}^{-z^2}\\ +\sqrt{\pi}\mathrm{Erf}\,(z)\end{aligned} \tag{B18}$$

$$\begin{aligned}\mathrm{h}(z_1,z_2)=2\frac{z_1^2-z_1z_2+z_2^2-2}{z_1^3+z_2^3}\mathrm{e}^{-\frac{1}{4}(z_1+z_2)^2}\\ +\sqrt{\pi}\mathrm{Erf}\left(\frac{z_1+z_2}{2}\right)\\ -2\frac{z_1^2+z_1z_2+z_2^2-2}{z_1^3+z_2^3}\mathrm{e}^{-\frac{1}{4}(z_1-z_2)^2}\\ -\sqrt{\pi}\frac{z_1^3-z_2^3}{z_1^3+z_2^3}\mathrm{Erf}\left(\frac{z_1-z_2}{2}\right)\end{aligned} \tag{B19}$$

The latter function is related to the $\mathcal{W}^F$ function defined in Ref. [5] as

$$\mathcal{W}^F(k_1,k_2)=\frac{16\pi^{7/2}}{3}(k_1^3+k_2^3)\,\mathrm{h}(z_1,z_2) \tag{B20}$$

The other functions read

$$\begin{aligned}\mathrm{u}(z,z_F)=\frac{1}{z}\left[\mathrm{e}^{-\frac{1}{4}(z+z_F)^2}-\mathrm{e}^{-\frac{1}{4}(z-z_F)^2}\right]\\ +\frac{\sqrt{\pi}}{2}\left[\mathrm{Erf}\left(\frac{z+z_F}{2}\right)-\mathrm{Erf}\left(\frac{z-z_F}{2}\right)\right]\end{aligned} \tag{B21}$$

$$\mathrm{u}_1(z,z_F)=-\frac{z_F^2}{2z}\left[\mathrm{e}^{-\frac{1}{4}(z+z_F)^2}-\mathrm{e}^{-\frac{1}{4}(z-z_F)^2}\right] \tag{B22}$$

$$\begin{aligned}\mathrm{m}(z,z_F)=\frac{1}{4z^3}\Big\{(2-zz_F)\mathrm{e}^{-\frac{1}{4}(z-z_F)^2}\\ -(2+zz_F)\mathrm{e}^{-\frac{1}{4}(z+z_F)^2}\Big\}\end{aligned} \tag{B23}$$

Note that in Ref. [12] a factor of 1/2 is missing.

$$\mathrm{p}(z)=-\frac{1}{z^3}+\frac{1}{2z}+\left(\frac{1}{z^3}+\frac{1}{2z}\right)\mathrm{e}^{-z^2} \tag{B24}$$

$$\mathrm{k}(z)=-\frac{6}{z^3}+\frac{2}{z}+\left(\frac{6}{z^3}+\frac{4}{z}+z\right)\mathrm{e}^{-z^2} \tag{B25}$$

$$\mathrm{q}(z)=-\frac{54}{z^3}+\frac{14}{z}+\left(\frac{54}{z^3}+\frac{40}{z}+13z+2z^3\right)\mathrm{e}^{-z^2} \tag{B26}$$

We notice that in Ref. [12] there is a missprint in Eq. B10.

$$\mathrm{s}_1(z)=\frac{1}{z}-\left(z+\frac{1}{z}\right)\mathrm{e}^{-z^2} \tag{B27}$$

$$\mathrm{s}_2(z)=-z+\frac{1}{z}-\frac{1}{z}\mathrm{e}^{-z^2} \tag{B28}$$

$$\mathrm{l}_1(z) = -\frac{1}{z} + \left(\frac{1}{z} + z + 2z^3\right)\mathrm{e}^{-z^2} \tag{B29}$$

$$\mathrm{l}_2(z) = -\frac{1}{z} - z + \left(\frac{1}{z} + 2z\right)\mathrm{e}^{-z^2} \tag{B30}$$

$$\mathrm{k}_1(z) = -\frac{1}{z} + \left(\frac{1}{z} + z + \frac{z^3}{2} + z^5\right)\mathrm{e}^{-z^2} \tag{B31}$$

$$\mathrm{k}_2(z) = -\frac{1}{z} - \frac{z}{2} + \left(\frac{1}{z} + \frac{3z}{2} + z^3\right)\mathrm{e}^{-z^2} \tag{B32}$$

$$\mathrm{q}_1(z) = -\frac{14}{z} + \left(\frac{14}{z} + 14z + 7z^3 + 4z^5 + 4z^7\right)\mathrm{e}^{-z^2} \tag{B33}$$

$$\mathrm{q}_2(z) = -\frac{14}{z} - 5z + \left(\frac{14}{z} + 19z + 12z^3 + 4z^5\right)\mathrm{e}^{-z^2} \tag{B34}$$

Appendix C Finite-range density-dependent D2 interaction

In Ref. [32], the Skyrme-like zero-range density-dependent term entering Gogny interaction, was replaced by a finite-range one of the form

$$\left\{W_d + B_d P_\sigma - H_d P_\tau - M_d P_{\sigma,\tau}\right\} \frac{\rho^\alpha}{(\mu_d\sqrt{\pi})^3}\,\mathrm{e}^{-r_{12}^2/\mu_d^2}. \tag{C1}$$

We define the combinations

$$A_0^d = \frac{1}{4}(4W_d + 2B_d - 2H_d - M_d) \tag{C2}$$

$$A_1^d = \frac{1}{4}(-2H_d - M_d) \tag{C3}$$

$$B_{nn}^d = -\frac{1}{\mu_d^3\pi^2}(W_d + 2B_d - H_d - 2M_d) \tag{C4}$$

$$B_{np}^d = \frac{1}{\mu_d^3\pi^2}(H_d + 2M_d) \tag{C5}$$

$$B_0^d = B_{nn}^d + B_{np}^d \tag{C6}$$

$$B_1^d = B_{nn}^d - B_{np}^d \tag{C7}$$

We define the dimensionless quantity $x^d = \mu_d k$ and the subindex F refers to the Fermi momentum. The functions u, m, g, h, etc. are the same as before.

The following contributions should be added to the different quantities defined in the text

- single-particle potential

$$\begin{aligned} U_\tau(D2) \leftarrow\ & A_0^d\rho^{\alpha+1} + A_1^d\tau\beta\rho^{\alpha+1} \\ & + \rho^\alpha B_{nn}^d \mathrm{u}(x^d, x_\tau^d) + \rho^\alpha B_{np}^d \mathrm{u}(x^d, x_{-\tau}^d)) \\ & + \frac{1}{2}\alpha\left[\frac{1}{2}\left(A_0^d + A_1^d\beta^2\right)\rho^{\alpha+1}\right. \\ & + \frac{1}{4}\rho^\alpha B_{nn}^d\left[(1+\beta)\mathrm{g}(x_n^d) + (1-\beta)\mathrm{g}(x_p^d)\right] \\ & \left. + \frac{1}{2}\rho^\alpha B_{np}^d \mathrm{h}(x_n^d, x_p^d)\right] \end{aligned} \tag{C8}$$

- isoscalar potential

$$\begin{aligned} U_0(D2) \leftarrow\ & A_0^d\rho^{\alpha+1} + B_0^d\rho^\alpha \mathrm{u}(x^d, x_F^d) \\ & + \frac{1}{4}\alpha\left[A_0^d\rho^{\alpha+1} + \rho^\alpha B_0^d \mathrm{g}(x_F^d)\right] \end{aligned} \tag{C9}$$

- isovector potential

$$U_1(D2) \leftarrow A_1^d\rho^{\alpha+1} + \frac{1}{3}\rho^\alpha B_1^d \mathrm{u}_1(x_F^d) \tag{C10}$$

Note that the rearrangement contribution (term proportional to α in Eq. C8), cancels out exactly in this case.

- effective mass

$$\frac{\hbar^2}{2m_\tau^*} \leftarrow \rho^\alpha\mu_d^2\left(B_{nn}^d \mathrm{m}(x^d, x_\tau^d) + B_{np}^d \mathrm{m}(x^d, x_{-\tau}^d)\right) \tag{C11}$$

- energy per particle in asymmetric nuclear matter

$$\begin{aligned} e_{ANM} \leftarrow\ & \frac{1}{2}\left(A_0^d + A_1^d\beta^2\right)\rho^{\alpha+1} \\ & + \frac{1}{4}\rho^\alpha B_{nn}^d\left[(1+\beta)\mathrm{g}(x_n^d) + (1-\beta)\mathrm{g}(x_p^d)\right] \\ & + \frac{1}{2}\rho^\alpha B_{np}^d \mathrm{h}(x_n^d, x_p^d) \end{aligned} \tag{C12}$$

- quantities relevant in symmetric nuclear matter

$$e_{SNM} \leftarrow \frac{1}{2}A_0^d\rho^{\alpha+1} + \frac{1}{2}\rho^\alpha B_0^d \mathrm{g}(x_F^d) \tag{C13}$$

$$\begin{aligned} P_{SNM} \leftarrow\ & \frac{1}{2}(\alpha+1)A_0^d\rho^{\alpha+2} \\ & + \rho^{\alpha+1}B_0^d\left(\frac{1}{2}\alpha\mathrm{g}(x_F^d) + \mathrm{p}(x_F^d)\right) \end{aligned} \tag{C14}$$

$$\begin{aligned} K_0 \leftarrow\ & \frac{9}{2}\alpha(\alpha+1)\rho^{\alpha+1}A_0^d \\ & - 3B_0^d\rho^\alpha\left\{-\frac{3}{2}\alpha(\alpha-1)\mathrm{g}(x_F^d)\right. \\ & \left. - 6\alpha\mathrm{p}(x_F^d) + \mathrm{k}(x_F^d)\right\} \end{aligned} \tag{C15}$$

$$\begin{aligned} Q_0^d \leftarrow\ & \frac{27}{2}\alpha(\alpha^2-1)\rho^{\alpha+1}A_0^d \\ & + 3B_0^d\rho^\alpha\left\{\frac{9}{2}\alpha(\alpha-1)(\alpha-2)\mathrm{g}(x_F^d)\right. \\ & \left. + \alpha(27\alpha-43)\mathrm{p}(x_F^d) - \alpha\mathrm{k}(x_F^d) + \mathrm{q}(x_F^d)\right\} \end{aligned} \tag{C16}$$

- quantities relevant in pure neutron matter

$$e_{PNM} \leftarrow \frac{1}{2}\left(A_0^d + A_1^d\right)\rho^{\alpha+1} + \frac{1}{2}\rho^\alpha B_{nn}^d \mathrm{g}(x_F^d) \quad \text{(C17)}$$

$$P_{PNM} \leftarrow \frac{1}{2}(\alpha+1)\left(A_0^d + A_1^d\right)\rho^{\alpha+2} + \rho^{\alpha+1} B_{nn}^d \left(\frac{1}{2}\alpha \mathrm{g}(x_F^d) + \mathrm{p}(x_F^d)\right) \quad \text{(C18)}$$

- isovector properties

$$S(\rho) \leftarrow \frac{1}{2}A_1^d\rho^{\alpha+1} + \frac{1}{6}\rho^\alpha B_{nn}^d \mathrm{s}_1(x_F^d) + \frac{1}{6}\rho^\alpha B_{np}^d \mathrm{s}_2(x_F^d) \quad \text{(C19)}$$

$$L(\rho) \leftarrow \frac{3}{2}A_1^d\rho^{\alpha+1} + \frac{1}{6}\rho^\alpha B_{nn}^d \mathrm{l}_1(x_F^d) + \frac{1}{6}\rho^\alpha B_{np}^d \mathrm{l}_2(x_F^d) + \frac{3}{2}\alpha A_1^d\rho^{\alpha+1} + \frac{1}{2}\alpha\rho^\alpha\left[B_{nn}^d \mathrm{s}_1(x_F^d) + B_{np}^d \mathrm{s}_2(x_F^d)\right] \quad \text{(C20)}$$

$$K_{\mathrm{sym}} \leftarrow \frac{9}{2}\alpha(\alpha+1)A_1^d\rho^{\alpha+1} - \frac{2}{3}\rho^\alpha B_{nn}^d \mathrm{k}_1(x_F^d) - \frac{2}{3}\rho^\alpha B_{np}^d \mathrm{k}_2(x_F^d) + \frac{3}{2}\alpha(\alpha-1)\rho^\alpha\left[B_{nn}^d \mathrm{s}_1(x_F^d) + B_{np}^d \mathrm{s}_2(x_F^d)\right] + \alpha\rho^\alpha\left[B_{nn}^d \mathrm{l}_1(x_F^d) + B_{np}^d \mathrm{l}_2(x_F^d)\right] \quad \text{(C21)}$$

$$Q_{\mathrm{sym}} \leftarrow \frac{27}{2}\alpha(\alpha^2-1)A_1^d\rho^{\alpha+1} + \frac{1}{3}\rho^\alpha B_{nn}^d \mathrm{q}_1(x_F^d) + \frac{1}{3}\rho^\alpha B_{np}^d \mathrm{q}_2(x_F^d) - 3\alpha\rho^\alpha\left[B_{nn}^d \mathrm{k}_1(x_F^d) + B_{np}^d \mathrm{k}_2(x_F^d)\right] + \frac{9}{2}\alpha(\alpha-1)\rho^\alpha\left[B_{nn}^d \mathrm{l}_1(x_F^d) + B_{np}^d \mathrm{l}_2(x_F^d)\right] + \frac{9}{2}\alpha(\alpha-1)(\alpha-2)\rho^\alpha\left[B_{nn}^d \mathrm{s}_1(x_F^d) + B_{np}^d \mathrm{s}_2(x_F^d)\right] \quad \text{(C22)}$$

References

1. M. Bender, P.-H. Heenen, P.-G. Reinhard, Rev. Mod. Phys. **75**, 121 (2003)
2. M. Grasso, Progr. Part. Nucl. Phys. **106**, 256 (2019)
3. T. Skyrme, Nucl. Phys. **9**, 615 (1958)
4. J. Dechargé, D. Gogny, Phys. Rev. C **21**, 1568 (1980)
5. H. Nakada, Phys. Rev. C **68**, 014316 (2003)
6. A. Bulgac, Y. Yu, Phys. Rev. Lett. **88**, 042504 (2002)
7. M. Kortelainen, T. Lesinski, J. Moré, W. Nazarewicz, J. Sarich, N. Schunck, M. Stoitsov, S. Wild, Phys. Rev. C **82**, 024313 (2010)
8. J. Dobaczewski, W. Nazarewicz, P. Reinhard, J. Phys. G: Nucl. Part. Phys. **41**, 074001 (2014)
9. N. Chamel, P. Haensel, Living Rev. Relativ. **11**, 1 (2008)
10. H. Hergert, Frontiers in Physics **8**, 379 (2020)
11. J. Erler, N. Birge, M. Kortelainen, W. Nazarewicz, E. Olsen, A.M. Perhac, M. Stoitsov, Nature **486**, 509 (2012)
12. R. Sellahewa, A. Rios, Phys. Rev. C **90**, 054327 (2014)
13. D. Davesne, P. Becker, A. Pastore, J. Navarro, Phys. Rev. C **93**, 064001 (2016)
14. D. Davesne, A. Pastore, J. Navarro, Progr. Part. Nucl. Phys. **120**, 103870 (2021)
15. G. Bertsch, J. Borysowicz, H. McManus, W. Love, Nucl. Phys. A **284**, 399 (1977)
16. N. Anantaraman, H. Toki, and Bertsch. Nucl. Phys. A **398**, 269 (1983)
17. D. Khoa, W. Oertzen, Phys. Lett. B **304**, 8 (1993)
18. D. Khoa, W. Oertzen, A. Ogloblin, Nucl. Phys. A **602**, 98 (1996)
19. D.T. Khoa, G.R. Satchler, W. von Oertzen, Phys. Rev. C **56**, 954 (1997). https://doi.org/10.1103/PhysRevC.56.954
20. D.T. Loan, N.H. Tan, D.T. Khoa, J. Margueron, Phys. Rev. C **83**, 065809 (2011)
21. H.S. Than, D.T. Khoa, N.V. Giai, Phys. Rev. C **80**, 064312 (2009). https://doi.org/10.1103/PhysRevC.80.064312
22. H. Nakada, Phys. Rev. C **78**, 054301 (2008)
23. H. Nakada, Phys. Rev. C **81**, 027301 (2010)
24. H. Nakada, Phys. Rev. C **87**, 014336 (2013)
25. H. Nakada, K. Sugiura, Progress of Theoretical and Experimental Physics **2014**, 033D02 (2014)
26. H. Nakada, T. Inakura, Phys. Rev. C **91**, 021302 (2015)
27. H. Nakada, K. Takayama, Phys. Rev. C **98**, 011301 (2018)
28. H. Nakada, K. Ishida, Phys. Rev. C **109**, 044614 (2024)
29. D.M. Brink, R.A. Broglia, Nuclear superfluidity: pairing in finite systems (Cambridge University Press, 2005)
30. M. Farine, D. Von-Eiff, P. Schuck, J. Berger, J. Dechargé, M. Girod, J. Phys. G: Nucl. Part. Phys. **25**, 863 (1999)
31. X. Viñas, C. González Boquera, M. Centelles, C. Mondal, L. M. Robledo Martín, Acta Physica Polonica B Proceedings Supplement **12**, 705 (2019)
32. F. Chappert, N. Pillet, M. Girod, J.-F. Berger, Phys. Rev. C **91**, 034312 (2015)
33. L. Batail, D. Davesne, S. Péru, P. Becker, A. Pastore, J. Navarro, Eur. Phys. J. A **59**, 173 (2023)
34. L. Batail, S. Goriely, S. Péru, S. Hilaire, D. Davesne, A. Pastore, to be published (2024)
35. M. Dutra, O. Lourenço, J.S. Martins, A. Delfino, J.R. Stone, P. Stevenson, Phys. Rev. C **85**, 035201 (2012)
36. B. Friedman, V. Pandharipande, Nucl. Phys. A **361**, 502 (1981)
37. A. Akmal, V. Pandharipande, R. Ravenhall, Phys. Rev. C **58**, 1804 (1998)
38. F. Chappert, M. Girod, S. Hilaire, Phys. Lett. B **668**, 420 (2008)
39. F. Mercier, J.-P. Ebran, E. Khan, Phys. Rev. C **107**, 034309 (2023)
40. X.-H. Li, W.-J. Guo, B.-A. Li, L.-W. Chen, F.J. Fattoyev, W.G. Newton, Phys. Lett. B **743**, 408 (2015)
41. M. Baldo, G. Burgio, H.-J. Schulze, G. Taranto, Phys. Rev. C **89**, 048801 (2014)
42. B.-A. Li, B.-J. Cai, L.-W. Chen, J. Xu, Progr. Part. Nucl. Phys. **99**, 29 (2018)
43. J. Rikovska Stone, J.C. Miller, R. Koncewicz, P.D. Stevenson, M.R. Strayer, Phys. Rev. C **68**, 034324 (2003). https://doi.org/10.1103/PhysRevC.68.034324
44. P. Danielewicz, R. Lacey, W.G. Lynch, Science **298**, 1592 (2002)
45. U. Garg, G. Colo, Progr. Part. Nucl. Phys. **101**, 55 (2018)
46. D. Youngblood, H. Clark, Y.-W. Lui, Phys. Rev. Lett. **82**, 691 (1999)
47. P. Veselỳ, J. Toivanen, B. Carlsson, J. Dobaczewski, N. Michel, A. Pastore, Phys. Rev. C **86**, 024303 (2012)
48. J. Piekarewicz, Phys. Rev. C **76**, 031301 (2007)

49. M. Ferreira, C. Providência, Phys. Rev. D **104**, 063006 (2021)
50. J. Margueron, F. Gulminelli, Phys. Rev. C **99**, 025806 (2019)
51. E. Khan, Phys. Scr. **2013**, 014008 (2013)
52. R. J. Barlow, Statistics: a guide to the use of statistical methods in the physical sciences, vol. 29 (John Wiley & Sons, 1993)
53. N. Chamel, P. Haensel, Living Rev. Relativ. **11**, 1 (2008)
54. C. Drischler, K. Hebeler, A. Schwenk, Phys. Rev. Lett. **122**, 042501 (2019)
55. A.L. Watts, N. Andersson, D. Chakrabarty, M. Feroci, K. Hebeler, G. Israel, F.K. Lamb, M.C. Miller, S. Morsink, F. Özel et al., Rev. Mod. Phys. **88**, 021001 (2016)
56. S. Greif, G. Raaijmakers, K. Hebeler, A. Schwenk, A. Watts, MNRAS **485**, 5363 (2019)
57. N. K. Glendenning, Compact stars: Nuclear physics, particle physics and general relativity (Springer Science & Business Media, 2012)
58. J.M. Lattimer, A.W. Steiner, Eur. Phys. J. A **50**, 1 (2014)
59. Y. Zhou, L.-W. Chen, Astrophys. J. **886**, 52 (2019)
60. P. Danielewicz, J. Lee, Nucl. Phys. A **922**, 1 (2014)
61. M. Centelles, X. Roca-Maza, X. Vinas, M. Warda, Phys. Rev. Lett. **102**, 122502 (2009)
62. B.-A. Li, B.-J. Cai, W.-J. Xie, N.-B. Zhang, Universe **7**, 182 (2021)
63. D. Adhikari, H. Albataineh, D. Androic, K. Aniol, D. Armstrong, T. Averett, C.A. Gayoso, S. Barcus, V. Bellini, R. Beminiwattha et al., Phys. Rev. Lett. **126**, 172502 (2021)
64. B.T. Reed, F.J. Fattoyev, C.J. Horowitz, J. Piekarewicz, Phys. Rev. Lett. **126**, 172503 (2021)
65. C. Mondal, B.K. Agrawal, J.N. De, S.K. Samaddar, M. Centelles, X. Viñas, Phys. Rev. C **96**, 021302 (2017). https://doi.org/10.1103/PhysRevC.96.021302
66. D. Davesne, J. Navarro, J. Meyer, K. Bennaceur, A. Pastore, Phys. Rev. C **97**, 044304 (2018)
67. D. Davesne, A. Pastore, J. Navarro, Astron. Astrophys. **585**, A83 (2016)
68. C. Gonzalez-Boquera, M. Centelles, X. Viñas, A. Rios, Phys. Rev. C **96**, 065806 (2017)
69. P. Haensel, Space Sci. Rev. **74**, 427 (1995)
70. J.M. Lattimer, C.J. Pethick, M. Prakash, P. Haensel, Phys. Rev. Lett. **66**, 2701 (1991). https://doi.org/10.1103/PhysRevLett.66.2701
71. D. Blaschke, H. Grigorian, D. Voskresensky, F. Weber, Phys. Rev. C **85**, 022802 (2012)
72. F.J. Fattoyev, J. Piekarewicz, Phys. Rev. C **86**, 015802 (2012)
73. F. Douchin, P. Haensel, Astron. Astrophys. **380**, 151 (2001)
74. M. Fortin, C. Providência, A.R. Raduta, F. Gulminelli, J. Zdunik, P. Haensel, M. Bejger, Phys. Rev. C **94**, 035804 (2016)
75. J. Antoniadis, P.C. Freire, N. Wex, T.M. Tauris, R.S. Lynch, M.H. Van Kerkwijk, M. Kramer, C. Bassa, V.S. Dhillon, T. Driebe et al., Science **340**, 1233232 (2013)
76. R.W. Romani, D. Kandel, A.V. Filippenko, T.G. Brink, W. Zheng, Astrophys. J. Lett. **934**, L18 (2022)
77. E. Annala, T. Gorda, A. Kurkela, A. Vuorinen, Phys. Rev. Lett. **120**, 172703 (2018)
78. P. Ring, P. Schuck, The nuclear many-body problem (Springer Science & Business Media, 2004)
79. V. Khodel, V. Khodel, J. Clark, Nucl. Phys. A **679**, 827 (2001)
80. C. Drischler, T. Krueger, K. Hebeler, A. Schwenk, Phys. Rev. C **95**, 024302 (2017)
81. S. Baroni, A.O. Macchiavelli, A. Schwenk, Phys. Rev. C **81**, 064308 (2010)
82. K. Hebeler, A. Schwenk, B. Friman, Phys. Lett. B **648**, 176 (2007)
83. E. Krotscheck, P. Papakonstantinou, J. Wang, Astrophys. J. **955**, 1 (2023)
84. A. Rios, A. Polls, W. Dickhoff, J. Low Temp. Phys. **189**, 234 (2017)
85. A. Sedrakian, T. Kuo, H. Müther, P. Schuck, Phys. Lett. B **576**, 68 (2003)
86. P. Borycki, J. Dobaczewski, W. Nazarewicz, M. Stoitsov, Phys. Rev. C **73**, 044319 (2006)
87. H. Nakada, M. Sato, Nucl. Phys. A **699**, 511 (2002)